2021

Aeolian Sand Stringers in the Upper Midwest, USA: Morphology, Stratigraphy, and Paleoenvironmental Significance

Kenzie L. Shandonay
Minnesota State University, Mankato

AEOLIAN SAND STRINGERS IN THE UPPER MIDWEST, USA:

MORPHOLOGY, STRATIGRAPHY, AND PALEOENVIRONMENTAL SIGNIFICANCE

By

Kenzie L. Shandonay

A Thesis Submitted in Partial Fulfillment of the

Requirements for the Degree of

Master of Science

In

Geography

Minnesota State University, Mankato

Mankato, Minnesota

May 2021

April 1st, 2021

Aeolian Sand Stringers in the Upper Midwest, USA: Morphology, Stratigraphy, and Paleoenvironmental Significance

Kenzie L. Shandonay

This thesis has been examined and approved by the following members of the student's committee.

_____

Dr. Mark Bowen

Primary Advisor

_____

Dr. Phillip Larson

Committee Member

_____

Dr. Garry Running

Committee Member

Acknowledgements

I cannot begin to express my appreciation for my advisor, Dr. Mark Bowen. He has provided me with invaluable guidance throughout this project, and his expertise has made me a better researcher, writer, geographer, and geomorphologist. It has been a great pleasure to work with him, and I am incredibly grateful to have him as a lifelong mentor. I also extend my utmost thanks to my committee members, Dr. Phil Larson and Dr. Garry Running. They have both provided essential knowledge, advice, and encouragement. I would also like to acknowledge my wonderful cohort. They have become exceptional friends who made Mankato feel like home.

I express my deepest gratitude to my family. My parents instilled in me a drive to work hard and follow my passions. In everything I do, they have always been my biggest fans. A sincere thank you also goes to my sister for her unwavering support.

Finally, I would like to extend my deepest appreciation and thanks to my husband, Ethan, who made sure to offer his help and support every step of the way. His humor, patience, understanding, and encouragement were paramount to the completion of my degree.

Funding

I am extremely grateful for the grants and scholarships I received which allowed me to fund my research. Many thanks to the donors of the James F. Goff Endowed Geography Graduate Research Award, the George J. Miller Endowed Geography Scholarship, and the Minnesota State University, Mankato Graduate Research Grant.

Table of Contents

List of Tables

List of Figures

Aeolian Sand Stringers in the Upper Midwest, USA:
Morphology, Stratigraphy, and Paleoenvironmental Significance
Kenzie L. Shandonay
A Thesis Submitted in Partial Fulfillment of the Requirements for the
Degree of Master of Science in Geography
Minnesota State University, Mankato
Mankato, Minnesota
May 2021

ABSTRACT

Sand stringers are subtle (~1-10 m high), elongate (several km long, up to 100 m wide) aeolian landforms that lack a slip face and generally have a northwest-southeast orientation. They are ubiquitous across the Upper Midwest, including southeast Minnesota and western Wisconsin. Despite their prevalence, the timing, processes, and environmental conditions during sand stringer formation and evolution are poorly understood. This research aims to describe sand stringer morphology and stratigraphy, reconstruct regional paleoclimate, and characterize the timing and geomorphic processes of sand stringer formation and evolution in response to shifts in environmental conditions.

This study investigates two sand stringers: Good-1 (Goodhue County, Minnesota) and ECC (Eau Claire County, Wisconsin). The morphology of each stringer was described using geospatial tools in ArcGIS. To obtain samples for analysis, a Giddings hydraulic soil coring machine was used to collect soil-sediment cores from Good-1 and ECC. Internal stratigraphy and paleoenvironmental conditions for each sand stringer were characterized by completing detailed soil profile descriptions and conducting particle size, magnetic susceptibility, and stable carbon isotope analyses. Optically stimulated luminescence (OSL) and radiocarbon dating provided age control for this study.

Good-1 and ECC morphology are comparable to other sand stringers described in the literature. Their northwest-southeast orientation indicates formation via northwesterly winds. Stratigraphy suggests sediment sources for Good-1 and ECC are different from one another. Good-1 is primarily composed of silt-rich, regional Peoria Loess, while ECC is primarily composed of sand derived from local sources. Timing of formation for the two sand stringers differ as well, with ages indicating Good-1 began forming following the Last Glacial Maximum (LGM) ~20-15 ka and ECC began forming during the Pleistocene-Holocene transition ~12-10 ka. Paleoenvironmental proxy data is consistent between the two stringers. Stable carbon isotopes generally decrease over time, indicating temperatures were colder than modern during sand stringer formation, and magnetic susceptibility data shows higher levels of pedogenic influence in the surface horizons, suggesting a prolonged period of stabilization and pedogenesis over the last several hundred to several thousand years. Outcomes from this research help expand the knowledge surrounding Midwestern aeolian systems and paleoenvironmental change since at least the LGM.

CHAPTER 1: INTRODUCTION

1.1. Introduction

Sand stringers, long and linear landforms, are ubiquitous aeolian deposits in the Upper Midwest. However, the timing, processes, and environmental conditions during sand stringer formation and evolution are poorly understood. To date, sand stringer studies have been limited (Zanner, 1999), leaving a large knowledge gap. The goal of this thesis is to gain a better understanding of sand stringer morphology, stratigraphy, and paleoenvironmental significance through a variety of field and laboratory methods. Chapter 1 includes a brief literature review, aimed at describing previous aeolian research, sand stringer research, and the importance of aeolian studies. Chapter 2 explores sand stringer morphology and stratigraphy by investigating soil cores from two different stringer sites. Chapter 3 examines proxy records of climate change from the same two stringers to determine whether stringers are useful archives of paleoenvironmental change. Finally, Chapter 4 summarizes the primary results, outcomes, and implications of this research, while also discussing future research approaches that can help advance the understanding of sand stringer formation, evolution, and environmental history of the Upper Midwest.

1.2. Aeolian Landforms in the Upper Midwest

Since the Last Glacial Maximum (LGM) ~26.5-19 ka (Clark et al., 2009), aeolian activity has helped shape the landscape of the Upper Midwest. Stabilized aeolian deposits (e.g., blowouts, climbing dunes, dune dammed drainages, loess deposits, parabolic dunes, sand ramps, sand sheets, sand stringers, etc.) have been identified across the region (e.g., Hanson et al., 2015; Mason et al., 1999; Rawling et al., 2008; Schaetzl et al., 2018, 2014; Stanley and Schaetzl, 2011; Zanner, 1999), indicating a past environment much different from today. By using a variety of geochronological and paleoenvironmental proxy methods, aeolian deposits across the Upper Midwest can reveal important information about the paleoclimate and vegetation history of the region (Schaetzl et al., 2018; Zanner, 1999).

During and following the LGM, aeolian deposits accumulated under varying wind regimes. The COHMAP (Cooperative Holocene Mapping Project) model projected a strong anticyclone off the southern margin of the Laurentide Ice Sheet, resulting in an easterly wind regime (COHMAP Members, 1988). This easterly flow has been confirmed from aeolian studies by Krist and Schaetzl (2001) and Vader et al. (2012), among others. However, several other studies of aeolian deposits have shown that winds during and following the LGM were dominantly from the west and northwest (Arbogast et al., 2015; Colgan et al., 2017; Rawling et al., 2008; Schaetzl et al., 2018).

The Pleistocene-Holocene transition and Early Holocene were periods of intense aeolian activity, as has been widely documented across the Upper Midwest (Fig. 1.1). In Northern Michigan, Krist and Schaetzl (2001) found lake spits with ages ~11-12 ka. In central and southern Michigan, dune field samples returned ages ~10-13 ka (Arbogast et al., 2015) and ~12-13 ka (Colgan et al., 2017). Studies from Wisconsin include Schaetzl et al. (2018) and Rawling et al. (2008), where sand ramp samples returned ages of ~10-11 ka and dune field samples returned ages ~11-14 ka, respectively. Hanson et al. (2015) studied aeolian ridgetop soils in southeastern Minnesota and determined aeolian sand had been deposited ~10-12 ka.

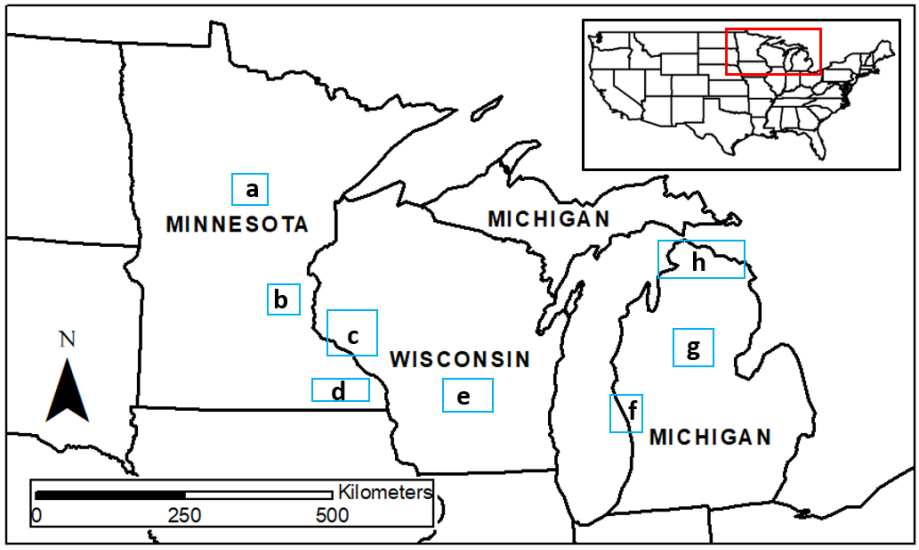

Figure 1.1. Map of some prior aeolian research locations. Blue boxes surround prior study areas: (a) Grigal et al. (1976), (b) Keen and Shane (1990), (c) Schaetzl et al. (2018) and Millett (2019), (d) Hanson et al. (2015), (e) Rawling et al. (2008), (f) Colgan at al. (2017), (g) Arbogast et al. (2015), and (h) Krist and Schaetzl (2001).

Although most studies from the Upper Midwest suggest aeolian activity primarily occurred during the Pleistocene-Holocene transition and Early Holocene, researchers have found evidence of more recent activity. A dune field in east-central Minnesota was determined to have started developing ~8 ka (Keen and Shane, 1990), and samples from a dune field in north-central Minnesota returned ages ~5-8 ka (Grigal et al., 1976). In west-central Wisconsin, samples from a cliff-top dune investigated by Schaetzl et al. (2018) also returned Middle Holocene ages of ~6-7 ka. Cliff top dune samples from western Wisconsin dated by Millett (2019) returned much younger, Late Holocene ages of ~0.4-1 ka.

These studies from the Upper Midwest suggest aeolian activity began by at least the LGM and persisted throughout most of the Holocene. The dominant wind direction was predominantly westerly to northwesterly; however, a large anticyclone off the Laurentide Ice Sheet resulted in an easterly wind regime along the ice margin. Many aeolian studies point to the Pleistocene-Holocene transition and Early Holocene as the periods with the most activity; however, other studies confirm that while aeolian activity may have declined, it continued in the Middle and Late Holocene.

1.3. Sand Stringers in the Upper Midwest

The term “sand stringer” was first used by McKee (1979) while studying aeolian landforms and deposits in the Sahara Desert and Arabian Desert. McKee (1979)

described sand stringers as linear sand features that lack a slip face and often develop downwind of a sand sheet. Zanner (1999) adopted the term “sand stringer” to describe stabilized, linear sand features he found in the Upper Midwest. Through remote mapping, he was able to identify sand stringers in parts of southern South Dakota, northern Iowa, southeast Minnesota, and northern Illinois.

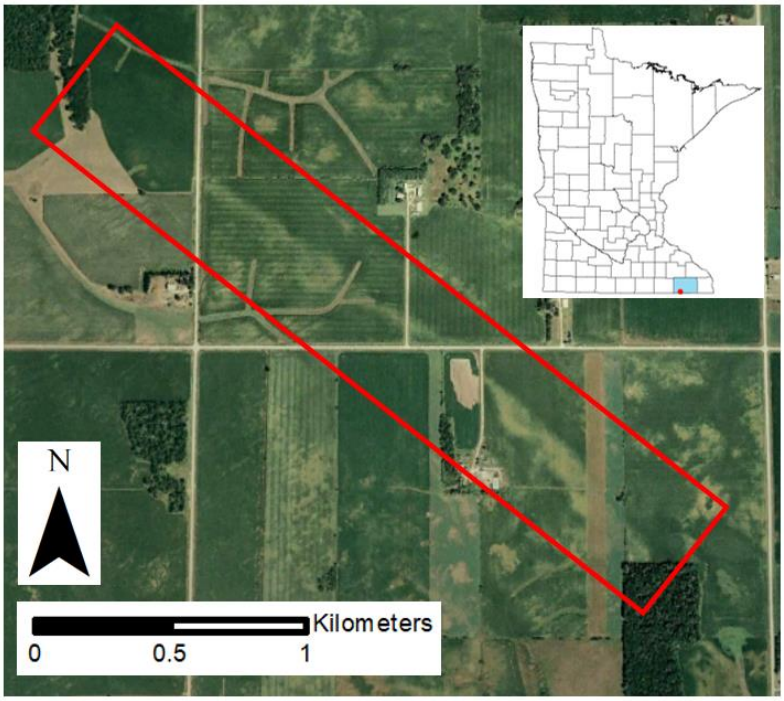

Figure 1.2. Map of the Canfield Creek stringer in Fillmore County, Minnesota (Zanner, 1999). The red box surrounds the sand stringer extent.

To better understand the significance of sand stringers across the region, Zanner (1999) conducted in-depth stratigraphic analysis at Canfield Creek stringer in Fillmore County, Minnesota (Fig. 1.2). Canfield Creek stringer is 2.3 km long and oriented

northwest-southeast, suggesting formation by northwest winds (Zanner, 1999). Thermoluminescence (TL) samples taken from depths of 81-150 cm at Canfield Creek stringer returned ages ~14.7-11.2 ka (Zanner, 1999). By excavating pits in Canfield Creek stringer and analyzing particle size, Zanner (1999) was able to identify fourteen stratigraphic units at this site.

At Canfield Creek stringer, sand wedges and solifluction features suggest the influence of permafrost on the landscape (Zanner, 1999). Based upon internal stratigraphy and TL ages, Zanner (1999) hypothesized that as permafrost melted following glacial retreat after the LGM, wind erosion began, continuing into the Early Holocene. Alternating layers of sand and silt within the stringer were interpreted to signify shifts in the position of the Des Moines Lobe (Zanner, 1999). Canfield Creek stringer provided no evidence of reactivation during the Middle or Late Holocene (Zanner, 1999).

More recently, sand stringers have been remotely mapped more broadly across northeast Iowa (Koch and Walters, 2004), southeast Minnesota (Marcou et al., 2019), and west-central Wisconsin (Millett et al., 2018; Schaetzl et al., 2018) (Fig. 1.3). Based on these remote mapping studies, sand stringers are typically ~1-10 m high, up to 100 m wide, and up to several km long. Sand stringers across the Upper Midwest exhibit the same northwest-southeast orientation determined by Zanner (1999).

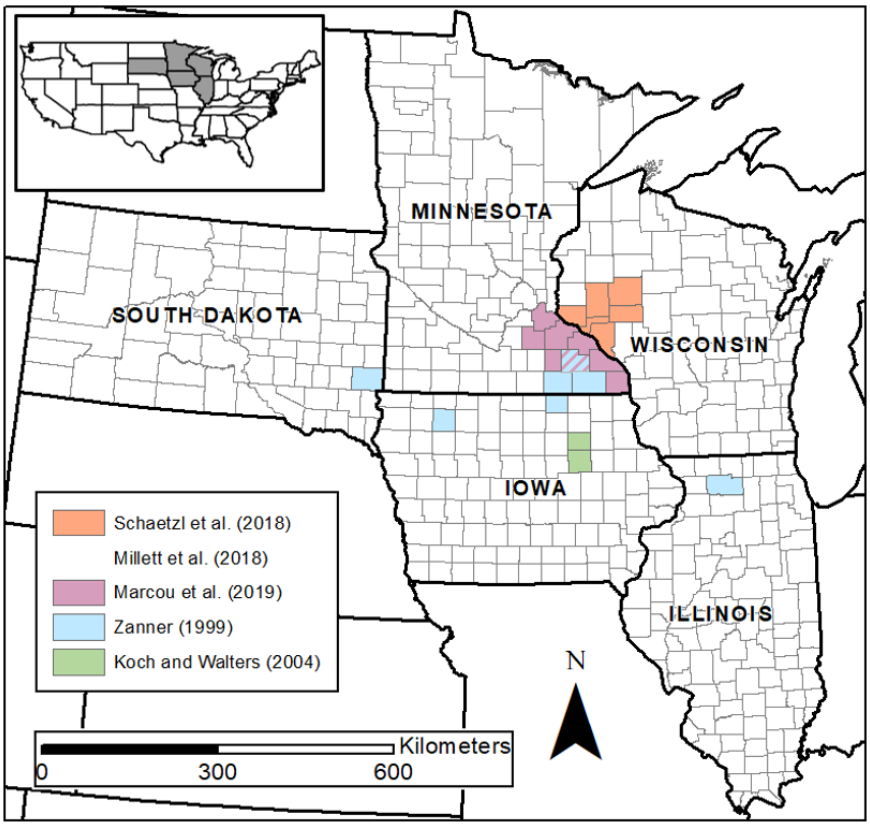

Figure 1.3. Map of states within the Upper Midwest, USA that have mapped or identified sand stringers. Counties are highlighted based upon the researcher(s) who identified sand stringers within them.

1.4. Importance of Aeolian Landforms in paleoclimate studies

Aeolian deposits can be important indicators of past environments, particularly climate, because aeolian processes are typically associated with a specific climate type (e.g., dry, sparse vegetation) (Muhs and Zárate, 2001; Zanner, 1999). The orientation of aeolian landforms can also indicate the dominant wind direction at the time of deposition (Muhs and Zárate, 2001; Zanner, 1999). Investigating morphology

and stratigraphy provides data useful for determining the formation and geomorphic evolution of aeolian deposits across a landscape (Muhs and Zárate, 2001; Pye and Tsoar, 2009; Schaetzl et al., 2018; Zanner, 1999).

Sand stringers in particular, are a ubiquitous aeolian landform of the Upper Midwest (Koch and Walters, 2004; Marcou et al., 2019; Millett et al., 2018; Schaetzl et al., 2018; Zanner, 1999), yet they have been investigated by few studies. The limited knowledge available suggests formation since the LGM (Zanner, 1999), indicating sand stringer research can provide valuable insight into the Midwestern paleoenvironment throughout at least the late Pleistocene and Holocene. The aim of this study is to build upon previous aeolian research within the Upper Midwest by analyzing the morphology, stratigraphy, and paleoenvironmental significance of two sand stringers in southeast Minnesota and western Wisconsin.

CHAPTER 2: MORPHOLOGY AND STRATIGRAPHY OF AEOLIAN SAND STRINGERS IN SOUTHEAST MINNESOTA AND WESTERN WISCONSIN

2.1. Introduction

Prior research has documented a variety of stabilized aeolian landforms and deposits (e.g., blowouts, climbing dunes, dune dammed drainages, loess deposits, parabolic dunes, sand ramps, sand sheets, sand stringers, etc.) throughout the landscapes of the Upper Midwest, USA (e.g., Hanson et al., 2015; Mason et al., 1999; Rawling et al., 2008; Schaetzl et al., 2018, 2014; Stanley and Schaetzl, 2011; Zanner, 1999), with deposition having occurred during and following the Last Glacial Maximum (LGM) 26.5-19 ka (Clark et al., 2009). In this prior research, aeolian deposits far removed from the former ice margin have orientations indicative of deposition by northwesterly winds (Keen and Shane, 1990; Mason et al., 1999; Rawling et al., 2008; Schaetzl et al., 2018; Stanley and Schaetzl, 2011).

One particular landform, sand stringers, are subtle, linear aeolian deposits, that have been identified in parts of South Dakota, Minnesota, Iowa, Wisconsin, and Illinois, USA (Koch and Walters, 2004; Marcou et al., 2019; Millett et al., 2018; Schaetzl et al., 2018; Zanner, 1999). A comprehensive analysis with modern geospatial datasets has not yet been completed, leaving the number of stringers and their true spatial distribution across this region not yet known. Those sand stringers that have been

identified have been described as ~1-10 m high, up to 100 m wide, and can reach several km in length (Koch and Walters, 2004; Mason et al., 1999; Millett et al., 2018; Schaetzl et al., 2018; Zanner, 1999). Unlike most sand dunes, sand stringers do not have an identifiable slip face (McKee, 1979; Zanner, 1999).

At present, Zanner (1999) is one of the few studies to comprehensively investigate the morphology, stratigraphy, and chronology of a sand stringer – Canfield Creek stringer in Fillmore County, Minnesota. Canfield Creek stringer is ~2.3 km in length and oriented northwest-southeast. Fourteen stratigraphic units were identified within Canfield Creek stringer (Fig. 2.1), and thermoluminescence ages of ~14.7-11.2 ka from depths of 81-150 cm within the younger aeolian sand and silt units were obtained. Zanner (1999) hypothesized that the stratigraphy within the stringer represented shifts in the position of the Des Moines Lobe. This remains the only hypothesis to explain the stratigraphy within a sand stringer. The limited scope of Zanner's (1999) investigation of only one sand stringer, and the use of a sometimes unreliable geochronology method (Noller et al., 2000) leaves the spatial distribution, environmental conditions during deposition, depositional chronology, and depositional processes of sand stringers still poorly understood across much of the Upper Midwest, USA. Given this, sand stringers in this region represent a relatively uninvestigated record of paleoenvironmental and geomorphic change post-LGM.

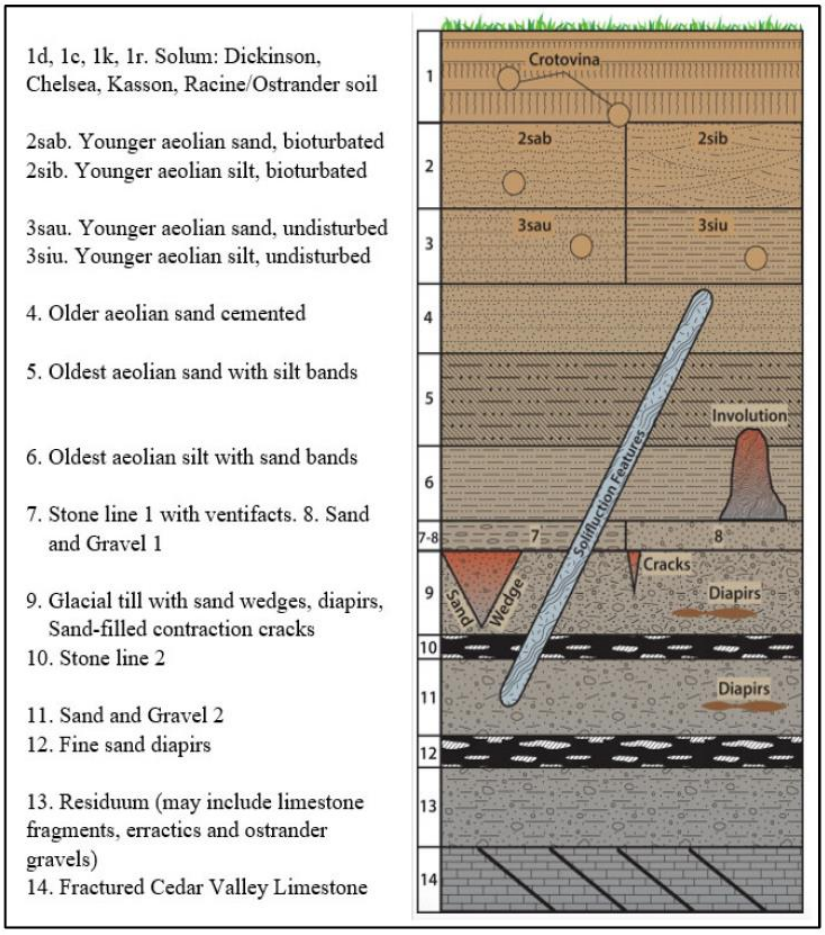

Figure 2.1. Simplified depiction of Canfield Creek stringer stratigraphy as described by Zanner (1999). Units 2 and 3 represent the body of the sand stringer.

The purpose of this research is to characterize sand stringer morphology and investigate the internal stratigraphy and sedimentology to reconstruct the timing and geomorphic processes of sand stringer formation and evolution in the Upper Midwest, USA. Objectives include: (1) calculating the morphometry (i.e., size and shape) of two sand stringers in the Upper Midwest using geographic information systems (GIS) and geospatial analysis techniques, (2) describing subsurface

stratigraphy by collecting soil-sediment cores and completing detailed soil profile/core descriptions, (3) characterizing particle size distribution for stratigraphic units using laser diffractometry techniques, and (4) determining the numerical age of stratigraphic units via radiocarbon and optically stimulated luminescence (OSL) dating.

2.2. Study Area

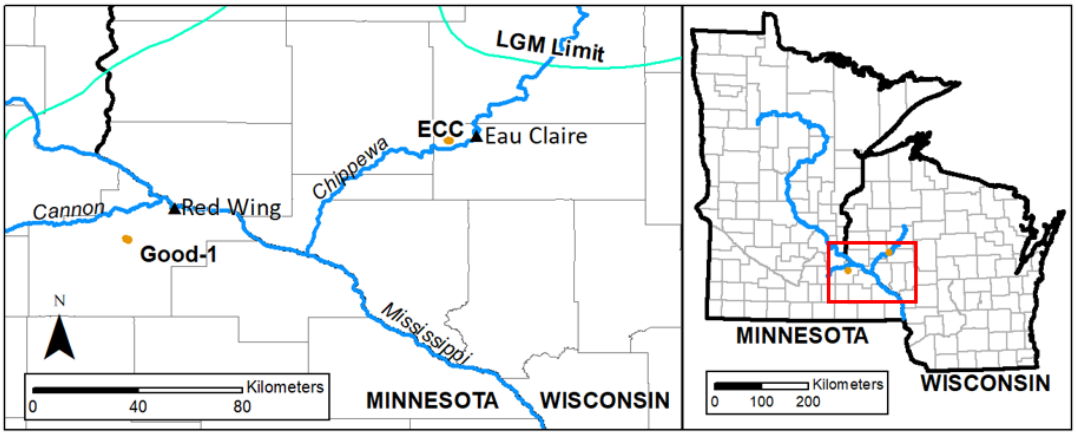

Figure 2.2. Location of Good-1 sand stringer in Goodhue County, Minnesota and ECC sand stringer in Eau Claire County, Wisconsin. LGM glacial ice limit at 18 ka from Dyke et al. (2003).

This project is focused on study sites located within Goodhue County, Minnesota (Good-1) and Eau Claire County, Wisconsin (ECC) (Fig. 2.2). Good-1 is located within an agricultural field on a broad, flat valley ~18 km southwest of Redwing, Minnesota, ~10 km south of the Cannon River, and ~18 km southwest of the Mississippi River (Figs. 2.2 and 2.3). ECC is located within an agricultural field on a broad upland ~8 km west of Eau

Claire, Wisconsin, ~3 km north of the Chippewa River, and ~60 km northeast of the Mississippi River (Figs. 2.2 and 2.3).

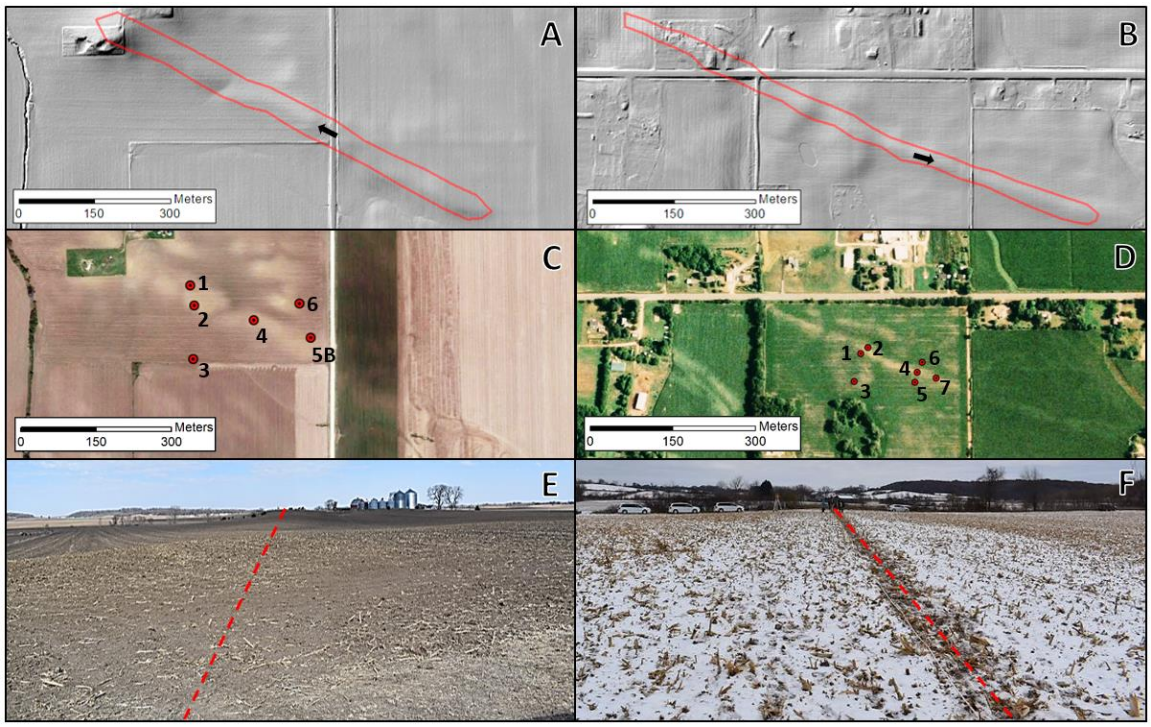

Figure 2.3. (a) Good-1 sand stringer LiDAR digital elevation model (DEM) with hillshade and stringer boundary, (b) ECC sand stringer LiDAR DEM with hillshade and stringer boundary, (c) Good-1 aerial imagery with coring locations, (d) ECC aerial imagery with coring locations, (e) Good-1 ground imagery looking northwest down the crest from the road immediately east of core 5B, and (f) ECC ground imagery looking southeast down the crest from immediately east of core 4.

Modern climate is similar between Goodhue and Eau Claire counties and can be characterized as having warm and wet summers with cold winters. The Köppen-Geiger climate classification for the study area is Dfb, which is indicative of a warm summer, humid continental climate (Peel et al., 2007). Based on 1981-2010 normals, average

annual temperature in Red Wing, Minnesota ranges from ~2-13°C, while average annual temperature in Eau Claire, Wisconsin ranges from ~1-13°C (U.S. Climate Data, 2020a, 2020b). In Red Wing, average annual precipitation is ~77.5 cm and average annual snowfall is ~81 cm, and in Eau Claire average annual precipitation is ~79 cm and average annual snowfall is ~119 cm (U.S. Climate Data, 2020a, 2020b). Most of the precipitation in the study area occurs as rain during summer convective thunderstorms (NRCS, 2006).

Good-1 is ~65 km east of the Des Moines Lobe terminal moraine boundary and ECC is ~50 km southwest of the Chippewa Lobe terminal moraine boundary. Glacial ice had left most of western Wisconsin, except for the Superior basin, between 16-11.4 ka (Clayton et al., 2001), and in southern Minnesota, Des Moines Lobe ice was present until ~14.1 ka (Clayton and Moran, 1982; Lepper et al., 2007). Zanner's (1999) study of the Canfield Creek sand stringer is the only investigation of sand stringers that includes geochronologic data. This work suggests that sand stringer deposition occurred sometime after the LGM, near the Pleistocene-Holocene transition ~14.7-11.2 ka. The Canfield Creek stringer, as well as Good-1 and ECC sites, are within the Driftless Area of the Interior Plains physiographic region (NRCS, 2006). The Driftless Area was not covered in glacial ice during the LGM, but was a landscape heavily influenced by permafrost conditions until ~13-12 ka (Clayton et al., 2001; Loope, 2012; Mason, 2015).

Local bedrock near Good-1 and ECC largely consists of Cambrian and Ordovician sandstone, dolomite, and shale with some limestone and siltstone (Jirsa et al., 2011; NRCS, 2006; University of Wisconsin - Extension, 2005). At Good-1, bedrock geology includes sandstone, dolostone and sandy dolostone (Runkel, 1998), while bedrock at ECC is sandstone (Brown, 1988). Peoria Loess, deposited 25-12 ka (Leigh and Knox, 1994), covers much of the bedrock in the study area (Anderson and Grigal, 1984; Jacobs et al., 1997; Muhs and Zárate, 2001; NRCS, 2006; Schaetzl et al., 2018). Loess is 1-8 m thick with a general decrease in thickness from west to east across the Midwest, though distribution can be variable (Mason et al., 1994; Muhs et al., 2008).

Paleovegetation studies have not been completed proximal to the study areas in Goodhue and Eau Claire counties; however, these data are available from central and northern Minnesota and northeastern Iowa. Following the LGM, the region was covered by tundra vegetation before transitioning to spruce dominated woodlands during the Pleistocene-Holocene transition, and then a mixed coniferous-deciduous forest during the Early Holocene (Birks, 1976; Chumbley et al., 1990; Grigal et al., 1976; Keen and Shane, 1990). During the Middle Holocene, prairie vegetation covered the region before being replaced with oak savanna in the Late Holocene (Chumbley et al., 1990; Keen and Shane, 1990). Modern vegetation within the study area is predominantly oak savanna with forests to the north and east and prairies to the south and west (Dunevitz and Epp, 1995; University of Wisconsin - Extension, 1965). The majority of the landscape has

been converted to cultivated cropland, with corn and soybeans being the most common (NRCS, 2006).

Soils within the study area are primarily classified as Alfisols, Entisols, and Mollisols with a mesic temperature regime (i.e., 8-15° C) and udic moisture regime (i.e., sufficient moisture to meet plant needs) (NRCS, 2006). Based on the U.S. Department of Agriculture Natural Resources Conservation Service (NRCS) Soil Survey Geographic Database (SSURGO 2.2) (Soil Survey Staff, 2019), Good-1 stringer soils are mapped as Mt. Carroll (Mollic Hapludalf), while soils surrounding the stringer are mapped as Barremills (Pachic Argiudoll) to the southwest and Port Byron (Typic Hapludoll) to the northeast. A typical Mt. Carroll soil is a silt loam with Ap-E-BE-Bt1-Bt2-Bt3-BC-C horizonation (Soil Survey Staff, 2011). Soil on the ECC stringer is mapped as Kevilar (Mollic Hapludalf), while Prissel (Arenic Hapludalf) and Meridan (Mollic Hapludalf) are mapped to the north-northeast and Ettrick (Fluvaquentic Endoaquoll) is mapped in a wetland to the southwest (Soil Survey Staff, 2019). A typical Kevilar soil is a sandy loam with Ap-Bt1-Bt2-2BC1-2BC2-3Bt horizonation with iron masses common in the 2BC2 and 3Bt horizons (Soil Survey Staff, 2001).

2.3. Methods

Morphology, stratigraphy, and age control for Good-1 and ECC were investigated using a combination of GIS, field, and laboratory work. GIS-based research included

digitizing each sand stringer boundary and calculating morphology. Using ArcMap 10.7.1, sand stringers were mapped via heads-up digitizing of boundaries visible on LiDAR-derived hillshade digital elevation models. LiDAR data for Goodhue and Eau Claire counties were acquired from the United States Department of Agriculture's National Resources Conservation Service Geospatial Data Gateway (https://datagateway.nrcs.usda.gov/). Good-1 and ECC stringer polygons were analyzed for a variety of morphological properties using ArcMap. The "measure" tool within ArcMap was used to determine the length and width of each sand stringer. Height of each sand stringer was determined using the "Spatial Analyst Extension" and the "Zonal Statistics" tool in ArcMap. The "Add Geometry" tool was used to determine the area and orientation of the long axis of each sand stringer. For orientation, the "Add Geometry" tool outputs a numerical bearing that can be used to determine cardinal direction for each sand stringer.

Field-based research involved using a Giddings hydraulic soil coring machine to collect six soil-sediment cores at Good-1 and seven soil-sediment cores at ECC (Tables 2.1 and 2.2; Figs. 2.3c and 2.3d). Cores were collected from a variety of landscape positions at both sites, including several cores along the crests and shoulders of the sand stringers and the valley floor adjacent to each stringer. Cores were collected to the maximum depth possible in 2.5-cm-diameter, clear, plastic liners, and capped, sealed, and transported to the EARTH Systems Laboratory at Minnesota State University,

Mankato for analysis. Core depth ranged from 145 cm to 313 cm at Good-1 and from 177 cm to 289 cm at ECC (Tables 2.1 and 2.2).

Table 2.1. Good-1 soil-sediment core information.

Good-1	Elevation (m)	Sand Stringer Geomorphic Position	Core Depth (cm)
1	313.55	South-east facing nose slope	282
2	312.16	Shoulder	241
3	310.06	Valley floor	145
4	313.25	Northwest-facing nose slope/swale	313
5B	317.79	Crest	199
6	316.43	Secondary peak	172

Table 2.2. ECC soil-sediment core information.

ECC	Elevation (m)	Sand Stringer Geomorphic Position	Core Depth (cm)
1	271.70	Crest	186
2	271.60	Shoulder	197
3	271.50	Valley floor	177
4	272.86	Crest	274
5	273.00	Shoulder	177
6	272.90	Shoulder	198
7	273.83	Crest	289

Laboratory methods employed for this investigation were soil core descriptions, particle size analysis, and age control via radiocarbon and OSL dating. All cores were described following standard U.S. Department of Agriculture National Soil Survey Center guidelines (Schoeneberger et al., 2012). Soil descriptions included horizonation, Munsell

color, structure, visible roots, visible rocks, boundary distinctness, consistence, hand texture, and redoximorphic features. Following core descriptions, samples were collected in 1-4 cm intervals, adjusted for stratigraphic complexity, for particle size analysis.

Particle size distribution was analyzed via laser diffraction techniques using a Malvern Mastersizer 3000. The Malvern Mastersizer outputs results in a range of 0.01-3500 µm by relative percent per size class distributed among 100 size classes. Laser diffraction analysis provides high-resolution particle size data that can be used to determine sand source and depositional process (Blott and Pye, 2006; Sun et al., 2002). Each sample was dried, ground using a mortar and pestle, and passed through a 2 mm sieve before being analyzed via wet dispersion. Enough sample was added to the dispersion unit to reach an obscuration of 5-10%, the sample was sonicated for 60 seconds, and particle size distribution was measured three times. An average was calculated for each sample, and sample average was used for analysis in this study. Between 34 and 121 samples were analyzed for each core and in total, 322 samples from Good-1 and 583 samples from ECC were analyzed. Particle class was determined using SEDCLASS, a program that generates a verbal equivalent to percent gravel, sand, silt, and clay based on the Shepard classification scheme (Poppe et al., 2003). Particle size distribution of individual samples from Good-1 and ECC was used to interpret geomorphic processes following Sun et al. (2002).

Age control for Good-1 and ECC was established via AMS radiocarbon dating of organic matter rich soils. Five samples from Good-1 at depths ranging from 118-235 cm and four samples from ECC at depths ranging from 61-128 cm were collected, dried, and ground and all visible roots and other debris were removed. Samples were then sealed in plastic vials and submitted to the National Ocean Sciences Accelerator Mass Spectrometry Lab (NOSAMS) for analysis. Radiocarbon ages were converted to calendar ages using the online CALIB 8.2 Radiocarbon Calibration Program (Stuiver et al., 2021). Optically stimulated luminescence (OSL) ages were obtained at ECC previously (Larson, pers. comm.). Four OSL samples were collected via bucket augering in opaque metal tubes at two points along the crest of ECC at depths ranging from 145-275 cm. Samples were submitted to the Utah State Luminescence Laboratory, and ages were acquired following the single-aliquot regenerative dose (SAR) method (Murray and Wintle, 2000). Both geochronological methods are useful in dating sand stringers as radiocarbon is effective for determining the age of organic-rich horizons while OSL is more suitable for sand-rich samples (Goble et al., 2004).

2.4. Results

2.4.1. Sand Stringer Morphology

Good-1 and ECC morphologies are similar to other sand stringers noted in prior literature (Koch and Walters, 2004; Mason et al., 1999; Millett et al., 2018; Schaetzl et

al., 2018; Zanner, 1999) and generally similar to each other. Good-1 is ~860 m long and 50-80 m wide, and ECC is ~945 m long and 30-50 m wide. Good-1 is slightly taller with a total relief of ~3-5 m from crest to valley floor along most of the crest; there is a pronounced peak ~10 m higher than the valley floor ~70 m from the northwest edge of the stringer and a pronounced swale ~1 m higher than the valley floor ~300 m from the northwest edge. ECC has a total relief of ~3-4 m from crest to valley floor, and the crest is relatively uniform and gently sloping with the valley floor to the northwest. Bearings for Good-1 and ECC are 117° and 112°, respectively, indicating the long axis of both sand stringers trends east-south-east.

2.4.2. Soil Core Descriptions

2.4.2.1. Good-1

Soil core descriptions for Good-1 reveal the main stringer body is composed of a ~150-270-cm- thick finer-grained unit with a well-developed surface soil (Fig. 2.4, Tables 2.3-2.8). The surface soil A horizon is 20-36 cm thick, dark brown, with granular or weak subangular blocky structure, and the upper ~15 cm has been disturbed by plowing. The B horizon is 18-29 cm thick with brown to dark yellowish brown color, subangular to angular blocky structure, and increased sand content. The B horizon is only weakly expressed along the sand stringer crest. Cores 1, 2, and 6 have a ~20-30-cm thick sandy loam to sandy clay loam BC horizon that is brown to dark yellowish brown with

subangular blocky structure. The C horizon is ~100-200 cm thick, yellowish brown to dark yellowish brown, with weak subangular blocky structure or is structureless. Few, very fine roots are restricted to the A horizon. Rocks and redoximorphic features are largely absent from this unit.

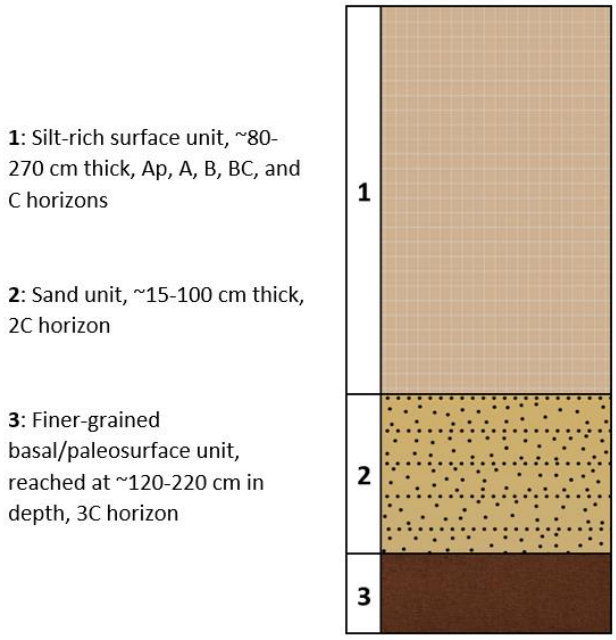

Figure 2.4. Simplified stratigraphy found at Good-1 stringer.

The finer-grained unit overlies structureless sand with iron staining and Fe-Mn nodules common, brown to yellow brown color, and very friable to loose consistence. Rocks and pebbles are distributed throughout the unit. At core 4, near the swale, the middle 50 cm of this unit is carbonate cemented. Carbonates were not observed in any other cores.

Core 3 was collected from the valley floor immediately adjacent to the sand stringer. The soil profile is composed of three distinct parent materials (Table 2.5). A 64-cm-thick sandy clay loam with Ap-A-AB horizonation overlies a 56-cm-thick sandy loam to sand unit with 2B-2C-2C2-2C3 horizonation and fine gravel throughout the 2B and 2C3 horizons. Underlying the sand is a very firm sandy clay loam with strong brown color, which was also identified in the base of core 2. This unit is interpreted as a paleosurface that pre-dates stringer formation.

Table 2.3. Soil profile description for Good-1 core 1

Depth (cm)	**Soil Horizon**	**Description**
0-15	Ap	7.5YR 3/2 (dark brown); silty clay to silty clay loam; strong, medium, granular structure; friable; clear horizon boundary
15-29	A	7.5YR 3/3 (dark brown); silty clay loam; moderate, medium granular structure; friable; clear horizon boundary
29-49	B	7.5 YR 3/4 (dark brown); sandy clay to sandy clay loam; moderate, fine to medium, angular blocky structure; very friable; gradual horizon boundary
49-71	BC	7.5YR 4/4 (brown); sandy loam; weak fine to medium subangular blocky structure; very friable; gradual horizon boundary
71-142	C stratified	10YR 4/4 (dark yellowish brown) and 10YR 6/4 (light yellowish brown); sandy loam with sand to loamy sand bedding; weak fine to medium subangular blocky structure; very friable; 1- to 3-cm-thick layers of slight iron staining throughout; gradual horizon boundary
142-267	C2	10YR 5/4 (yellowish brown); sandy loam; weak fine to medium subangular blocky structure; very friable; slight iron staining throughout; 1 cm pebble found at 240 cm; gradual horizon boundary
267-276	2C	10YR 5/4 (yellowish brown) and 10YR 7/4 (very pale brown); sandy loam; weak fine to medium subangular blocky structure; very friable; clear horizon boundary
276-282	2C2	10YR 7/4 (very pale brown); sand; weak fine to medium subangular blocky structure; very friable; 2 cm gravel at 276 cm

Table 2.4. Soil profile description for Good-1 core 2

Depth (cm)	Soil Horizon	Description
0-15	Ap	10YR 3/3 (dark brown); silt loam to loam; granular to subangular blocky structure; friable; few very fine roots throughout; abrupt horizon boundary
15-29	A	10YR 3/3 (dark brown); silt loam to loam; granular to subangular blocky structure; friable; very few very fine roots throughout; clear horizon boundary
29-49	B	10YR 3/4 (dark yellowish brown); silt loam; subangular blocky structure; friable; clear horizon boundary
49-79	BC	10YR 4/4 (dark yellowish brown); sandy clay loam; subangular blocky structure; friable; gradual horizon boundary
79-165	C	10YR 5/4 (yellowish brown); silty clay loam; subangular blocky structure; friable; gradual horizon boundary
165-190	C2	10YR 5/3 (brown); silty clay loam; weak subangular blocky structure; friable; clear horizon boundary
190-216	2C	10YR 5/4 (yellowish brown); silt loam to loam; weak subangular blocky structure; friable; fine gravel common (15-30%); abrupt horizon boundary
216-241	3C	7.5YR 4/4 (brown); sandy loam; weak subangular blocky structure; friable; 1 large stone and a few fine gravel

Table 2.5. Soil profile description for Good-1 core 3

Depth (cm)	Soil Horizon	Description
0-16	Ap	10YR 2/2 (very dark brown); sandy clay loam; subangular blocky structure; friable to firm; few very fine roots throughout; gradual horizon boundary
16-46	A	10YR 2/1 (black); sandy clay loam; subangular blocky structure; friable to firm; very few very fine roots throughout; clear horizon boundary
46-64	AB	10YR 3/2 (very dark grayish brown); sandy clay loam subangular blocky structure; friable to firm; clear horizon boundary
64-80	2B	10YR 4/4 (dark yellowish brown); sandy loam; subangular blocky structure; firm; fine gravel throughout; abrupt horizon boundary
80-101	2C	10YR 7/4 (very pale brown); sand; single grained; very friable to loose; clear shift to sand; abrupt horizon boundary
101-111	2C2	7.5YR 5/8 (strong brown); sand; single grained; very friable to loose; clear horizon boundary
111-120	2C3	7.5YR 6/8 (reddish yellow); sandy; massive; very firm; fine to medium gravel throughout; very dense and hard zone; abrupt horizon boundary
120-145	3C	7.5YR 4/6 (strong brown); sandy clay loam; granular to subangular blocky structure; very firm

Table 2.6. Soil profile description for Good-1 core 4

Depth (cm)	Soil Horizon	Description
0-15	Ap	10YR 2/2 (very dark brown); sandy clay loam; granular to subangular blocky structure; friable; very few very fine roots throughout; gradual horizon boundary
15-26	A	10YR 3/3 (dark brown); sandy clay loam; subangular blocky structure; friable; very few very fine roots throughout; clear horizon boundary
26-55	B	10YR 3/4 (dark yellowish brown); sandy loam; weak subangular blocky structure; very friable; gradual horizon boundary
55-116	C	10YR 5/4 (yellowish brown); silt loam; weak subangular blocky structure; very friable; gradual horizon boundary
116-214	C2	10YR 5/4 (yellowish brown); silty clay loam; weak subangular blocky structure; very friable; some carbonate; abrupt horizon boundary
214-233	2C	10YR 7/6 (yellow); sand; single grained; very friable; few gravel throughout; iron staining throughout; clear horizon boundary
233-283	2Ck	10YR 8/3 (very pale brown) to 10R 8/4 (pink); loamy sand; single grained; very friable; few gravel throughout; partly carbonate cemented; iron staining throughout; clear horizon boundary
283-313	2C2	10YR 7/6 (yellow); sand; single grained; very friable; iron staining throughout

Table 2.7. Soil profile description for Good-1 core 5B

Depth (cm)	Soil Horizon	Description
0-20	Ap	7.5YR 3/2 (dark brown); sandy clay to silty clay; weak to moderate granular structure; friable; very few very fine roots throughout; clear horizon boundary
20-58	B	7.5YR 4/3 (brown); sandy loam; structureless; loose to very friable; very few very fine roots throughout; diffuse horizon boundary
58-85	C	10YR 4/4 (dark yellowish brown); sandy loam to loamy sand; structureless; loose; very few very fine roots throughout; gradual horizon boundary
85-155	C2	10YR 4/4 (dark yellowish brown); silty clay loam; structureless; loose to very friable; very few very fine roots throughout; few pebbles in lower portion of this horizon; noticeable increase in fines; this horizon is much firmer than the rest; abrupt horizon boundary
155-199	2C	10YR 7/6 (yellow); sand; structureless; loose; distinct iron staining and manganese nodules throughout

Table 2.8. Soil profile description for Good-1 core 6

Depth (cm)	Soil Horizon	Description
0-16	Ap	10YR 2/2 (very dark brown); silty clay loam; granular structure; friable; very few very fine roots throughout; clear horizon boundary
16-36	A	10YR 3/3 (dark brown); silty clay loam; subangular blocky structure; friable; very few very fine roots throughout; gradual horizon boundary
36-54	B	10YR 3/4 (dark yellowish brown); silty clay loam; subangular blocky structure; friable; clear horizon boundary
54-84	BC	10YR 4/4(dark yellowish brown); sandy clay loam; weak subangular blocky structure; very friable; abrupt horizon boundary
84-172	2C	10YR 4/6 (dark yellowish brown); loamy sand; weak subangular blocky structure; very friable; gravelly to very gravelly

2.4.2.2. ECC

Soil core descriptions at ECC revealed four distinct stratigraphic units (Fig. 2.5, Tables 2.9-2.15). The upper ~60-100 cm of ECC is primarily composed of sandy loam with Ap-A-B/Bt-BC horizonation. The A horizon is 13-45 cm thick, dark brown to grayish brown, with granular or weak subangular blocky structure. The upper ~16 cm was disturbed by plowing. B horizon thickness ranges from 16 cm to 37 cm, with the thickest B horizons on the shoulder positions. B horizon color is brown to dark gray brown with subangular blocky structure. Few, very fine roots were found in A horizons, but roots were not observed in any other horizons. Rocks and redoximorphic features were largely absent from this upper unit.

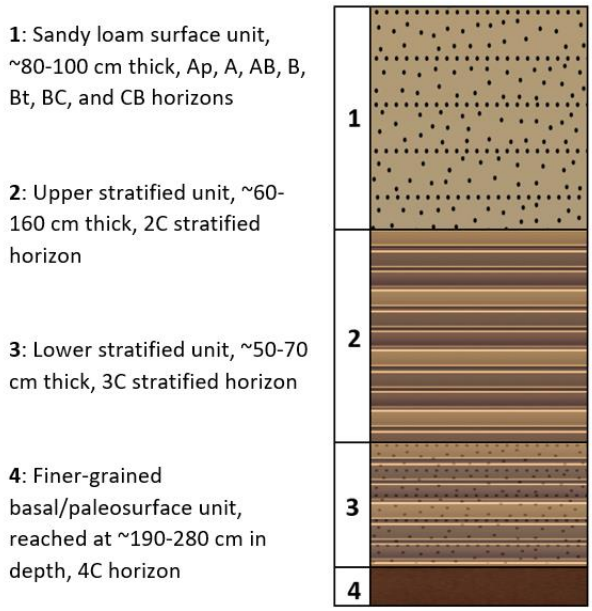

Figure 2.5. Simplified stratigraphy found at ECC stringer.

In all ECC cores, the sandy loam unit is underlain by a 60-160-cm-thick stratified loamy sand to sand unit with alternating 1-8-cm-thick iron-cemented sand and structureless sand beds. Contacts between beds are typically very abrupt with little to no gradation between them. Iron-cemented zones are dark brown with friable to firm consistence, while structureless sand zones are light brown or yellowish brown with loose consistence. Within cores 4, 5, 6, and 7 a second stratified sand unit was observed with evidence of gleying in cores 4, 5, and 7. Cores 4, 6, and 7 extended deep enough to encounter a fourth unit 190-280 cm deep, which was composed of a brown to very pale brown sandy loam with a sharp increase in silt and decrease in sand.

Table 2.9. Soil profile description for ECC core 1

Depth (cm)	**Soil Horizon**	**Description**
0-16	Ap	10YR 3/3 (dark brown); sandy loam; weak to moderate granular structure; very friable; very few very fine roots throughout; gradual horizon boundary
16-32	Bt	7.5YR 5/4 (brown) to 7.5YR 4/6 (strong brown); sandy clay loam to sandy clay; weak granular structure to structureless; very friable; very few very fine roots throughout; iron staining from 24-32 cm; abrupt horizon boundary
32-41	krotovina	7.5YR 3/3 (dark brown); sandy loam; structureless; very friable; abrupt horizon boundary
41-63	BC	7.5YR 5/4 (brown); loamy sand; structureless; very friable; abrupt horizon boundary; iron staining 7.5YR 3/4 (dark brown) from 56-63 cm
63-88	BC2	7.5YR 5/4 (brown); loamy sand to sand; structureless; loose; clear horizon boundary
88-186	2C stratified	7.5YR 4/4 (brown) to 7.5YR 6/4 (light brown); loamy sand to sand; structureless; loose to very friable; common 1- to 10-cm-thick iron staining (7.5YR 3/4; dark brown)

Table 2.10. Soil profile description for ECC core 2

Depth (cm)	Soil Horizon	Description
0-14	Ap	10YR 3/3 (dark brown); sandy loam; weak subangular blocky structure; very friable; few very fine roots throughout; gradual horizon boundary
14-24	A	10YR 3/3 (dark brown); sandy loam; weak subangular blocky structure; friable; few very fine roots throughout; diffuse horizon boundary
24-45	B	10YR 3/3 (dark brown); sandy loam; weak subangular blocky structure; very friable; few very fine roots throughout; gradual horizon boundary
45-97	BC	10YR 4/4 (dark yellowish brown) to 10YR 5/4 (yellowish brown); loamy sand; weak subangular blocky structure to structureless; very friable to loose; iron staining (7.5YR 3/4; dark brown to 7.5YR 4/4; brown) from 63-75 cm and 91-97 cm; clear horizon boundary
97-197	2C stratified	10YR 5/6 (yellowish brown) to 10YR 6/4 (light yellowish brown); loamy sand to sand; structureless; loose; iron staining (7.5YR 4/4; brown to 7.5YR 4/6; strong brown) from 105-107 cm, 121-132 cm, 152-157 cm

Table 2.11. Soil profile description for ECC core 3

Depth (cm)	Soil Horizon	Description
0-13	Ap	7.5YR 3/2 (dark brown); loam; weak to moderate medium subangular blocky structure; firm; few very fine roots throughout; diffuse horizon boundary
13-20	AB	7.5YR 4/4 (brown); clay loam; moderate to strong medium subangular blocky structure; firm to friable; few very fine roots throughout; mottled; diffuse horizon boundary
20-47	Bt	7.5YR 4/6 (strong brown); loamy sand; weak subangular blocky structure; friable; diffuse horizon boundary
47-59	BC	7.5YR 5/6 (strong brown); loamy sand; weak subangular blocky structure; very friable to loose; diffuse horizon boundary
59-91	CB	7.5YR 5/6 (strong brown); loamy sand; weak subangular blocky; very friable to loose; clear horizon boundary marked by 1-cm-thick iron staining
91-177	2C stratified	10YR 6/6 (brownish yellow); loamy sand to sand; weak subangular blocky structure to structureless; very friable to loose; iron staining (7.5YR 3/3; dark brown to 7.5YR 4/4; brown) at 91 cm, 106-109 cm, 125-128 cm, 142-144 cm, and 159-161 cm

Table 2.12. Soil profile description for ECC core 4

Depth (cm)	Soil Horizon	Description
0-15	Ap	10YR 5/2 (grayish brown) to 10YR 4/2 (brown); sandy loam; weak subangular blocky structure; friable; few very fine roots throughout; gradual horizon boundary
15-36	B	10YR 4/3 (brown); sandy loam; weak angular blocky structure; friable; few very fine roots throughout; gradual horizon boundary
36-84	BC	10YR 5/4 (yellowish brown); loamy sand; weak angular blocky structure to structureless; very friable; iron staining (7.5YR 3/4; dark brown) from 66-84; clear horizon boundary
84-194	2C stratified	7.5YR 4/6 (strong brown) and 10YR 5/6 (yellowish brown); loamy sand to sand; weak angular blocky to structureless; very friable to loose; iron staining and depletions throughout
194-264	3C stratified	10YR 6/4 (light yellowish brown); sand; structureless; loose; clear horizon boundary; iron staining at 196-200 cm, 203-204 cm, 211-217 cm, 233 cm, 256-258 cm, and 260-262 cm
264-274	4C	10YR 7.4 (very pale brown); sandy loam; weak subangular blocky structure; friable; iron staining from 267-269 cm

Table 2.13. Soil profile description for ECC core 5

Depth (cm)	Soil Horizon	Description
0-16	Ap	10YR 3/2 (very dark grayish brown); sandy loam; weak subangular blocky structure; friable; diffuse horizon boundary
16-58	Bt	10YR 4/2 (dark grayish brown); sandy clay loam; moderate to fine medium subangular blocky structure; friable; diffuse horizon boundary
58-71	BC	10YR 4/3 (brown); loamy sand; weak subangular blocky structure; friable; clear horizon boundary
71-130	2C stratified	10YR 3/6 (dark yellowish brown) and 10YR 7/1 (light gray); sandy loam; moderate to fine medium subangular blocky structure; firm to friable; alternating iron staining and depletion; clear horizon boundary
130-177	3C stratified	10YR 5/6 (yellowish brown); sand; weak subangular blocky structure to structureless; loose; iron staining (7.5YR 5/8; strong brown to 7.5YR 4/4; brown) from 131-138 cm, 146-149 cm, and 165-171 cm; small (<1 cm) gravels and pebbles from 138-153 cm

Table 2.14. Soil profile description for ECC core 6

Depth (cm)	Soil Horizon	Description
0-14	Ap	10YR 4/2 (dark grayish brown); sandy clay loam; weak angular blocky structure; friable; few very fine roots throughout; diffuse horizon boundary
14-40	B	10YR 3/2 (very dark grayish brown); sandy clay loam; weak angular blocky structure; friable; diffuse horizon boundary
40-57	BC	10YR 6/3 (pale brown); sandy clay loam; moderate subangular blocky structure; friable; clear horizon boundary
57-81	BC2	7.5YR 5/4 (brown; sandy loam; moderate subangular blocky structure; friable; iron staining (7.5YR 3/4; dark brown) from 78-81 cm
81-140	2C stratified	7.5YR 4/6 (strong brown) to 7.5YR 6/4 (light brown); loamy sand; weak subangular blocky structure to structureless; very friable; iron staining (7.5YR 3/4 to 7.5YR 3/3; dark brown) from 90-94 cm and 110-115
140-192	3C stratified	10YR 6/4 (light yellowish brown); sand; structureless; loose; clear horizon boundary; iron staining (7.5YR 3/4; dark brown to 7.5YR 5/4; brown) at 146 cm, 149-151 cm, 154-159 cm, 174-177 cm, and 190-191 cm
192-198	4C	10YR 6/3 (pale brown); sandy loam; weak subangular blocky structure to structureless; very friable

Table 2.15. Soil profile description for ECC core 7

Depth (cm)	Soil Horizon	Description
0-16	Ap	7.5YR 3/2 (dark brown); sandy loam; weak subangular blocky structure to structureless; loose to very friable; gradual horizon boundary
16-34	B	7.5YR 4/3 (brown); sandy loam; weak subangular blocky structure to structureless; loose to very friable; gradual horizon boundary
34-63	BC	7.5 YR 5/4 (brown); loamy sand; weak subangular blocky structure to structureless; loose to very friable; iron staining (5YR 4/4; reddish brown) from 57-63 cm; abrupt horizon boundary
63-112	2C stratified	7.5YR 5/4 (brown); loamy sand; weak subangular blocky structure to structureless; loose to very friable; abrupt horizon boundary
112-218	2C2 stratified	7.5YR 4/6 (strong brown) and 7.5YR 6/2 (pinkish gray); loamy sand and sandy clay loam to sandy clay; weak subangular blocky structure to structureless; loose to very friable; highly variable with depletions and iron staining; abrupt horizon boundary
218-280	3C stratified	7.5YR 6/4 (light brown); sand; structureless; loose; clear horizon boundary; iron staining (7.5YR 4/6; strong brown) at 232-233 cm, 242 cm, 254 cm, 275 cm, and 280 cm
280-289	4C	7.5YR 5/4 (brown); sandy loam; weak subangular blocky structure to structureless; loose to very friable

2.4.3. Particle Size

Particle size data reveal Good-1 is predominantly composed of silt, while ECC is predominantly composed of sand. Good-1 contained a fairly uniform silt-rich surface unit comprising the A, B, and C horizons that ranged from ~80 cm (core 6) to 270 cm (core 1) thick (Fig. 2.6). This upper unit is predominantly classified as clayey silt or loam in the Shepard system (Fig. 2.7). Median grain size (D50) ranges from 20-50 µm for most of the samples in this unit, which is silt in the USDA particle size class. Particle size percentages of sand, silt, and clay reveal this unit ranges from ~70-98% silt and clay.

Three of the six Good-1 cores have elevated sand percentages in the upper silt-rich unit: Core 1 from ~70 cm – 120 cm, core 4 from ~30 cm – 110 cm, and core 5B from ~40 cm – 80 cm (Fig. 2.6). The silt-rich unit was the thickest at cores 1, 2, and 4, thinner at cores 5B and 6, and thinnest on the valley floor at core 3. Samples taken from the base of the silt-rich unit returned radiocarbon ages of 25,440 ± 330 cal yrs BP at a depth of 216 cm in core 4 and 22,410 ± 100 cal yrs BP at 188 cm in core 2 (Table 2.16). Good-1 core 4 also returned an age of 9,140 ± 110 cal yrs BP from the base of the surface soil B horizon within the upper silt-rich unit.

Underlying the silt-rich surface unit at Good-1 is a sand-rich unit. This unit is primarily classified as sand, silty sand, or clayey sand in the Shepard system. Median grain size ranges from >50 μm to ~275 μm, which is in the sand USDA particle size class. Sand content ranges from ~50-98% in this lower unit. The sand unit is greater than 1 m thick at cores 4 and 6, but less than ~50 cm thick at cores 1, 2, 3, and 5B. The actual thickness of this sand-rich unit is unknown due to inability to penetrate deeper during coring. Below the sand, a clay-rich unit was captured within cores 2 and 3, which is interpreted as the paleosurface that pre-dates stringer formation. Samples collected near the top of this unit returned radiocarbon ages of 21,730 ± 300 cal yrs BP at 122 cm in core 3 and 20,120 ± 210 cal yrs BP at 235 cm in core 2. The returned age at 235 cm in core 2 is ~2,000 years younger than the returned age at 188 cm in core 2, which could be due to potential contamination by younger carbon. Reported radiocarbon ages are

generally younger than the actual soil age due to natural carbon cycling (Wang et al., 1996).

Grain size distributions of samples from the A, B, and C horizons within the upper silt-rich unit at Good-1 are bimodal (Fig. 2.8a). The primary peak is centered around ~30-50 µm (silt), and the secondary peak is centered around ~200-300 µm (fine to medium sand). Grain size distribution of the underlying sand unit is also bimodal (Fig. 2.8b), with a primary peak centered around ~200-300 µm and a secondary peak centered around ~20-50 µm. The bimodal distributions in both the upper and underlying units are fairly uniform across all Good-1 cores with the exception of core 5B. Grain size distributions are variable in the upper ~150 cm with bimodal and unimodal distributions centered around size classes ranging from 20 µm up to >1,000 µm (Fig. 2.9a). Although grain size distributions at Good-1 5B are irregular, silt-sized particles are still dominant above ~150 cm. Below ~150 cm, samples have a fairly uniform distribution centered around 200-300 µm with minor inputs from 2-50 µm (Fig. 2.9b).

*Table 2.16. Radiocarbon ages for Good-1 and ECC. Calendar ages calibrated using the online CALIB 8.2 Radiocarbon Calibration Program; ages rounded to the nearest decade. (*stratified horizon)*

Core Name	Depth (cm)	Soil Horizon	Lab Number	$\delta^{13}C$ (‰)	^{14}C age (yr BP ± 1σ)	Calendar age (yr BP ± 1σ)
ECC 1	61	BC	OS-159317	-21.30	1,410 ± 20	1,320 ± 20
ECC 7	91	2C strat*	OS-157918	-18.95	2,050 ± 20	1,990 ± 50
ECC 1	94	2C strat*	OS-157917	-19.84	5,470 ± 30	6,260 ± 40
ECC 1	128	2C strat*	OS-159383	-22.39	7,210 ± 35	8000 ± 30
Good-1 4	118	C2	OS-159319	-23.13	8,190 ± 30	9,140 ± 110
Good-1 3	122	3C	OS-158458	-19.92	17,900 ± 210	21,730 ± 300
Good-1 2	188	C2	OS-159318	-23.87	18,500 ± 110	22,410 ± 100
Good-1 4	216	2C	OS-158459	-24.31	21,100 ± 310	25,440 ± 330
Good-1 2	235	3C	OS-157919	-19.48	16,650 ± 160	20,120 ± 210

Table 2.17. OSL ages for ECC (Unpublished ages, Larson, pers. comm.)

Core Name (Larson, pers. comm.)	Core Name Equivalent	Depth (cm)	Num. of Aliqouts	Dose rate (Gy/ka)	Equivalent Dose ± 2σ (Gy)	OSL Age ± 2σ (ka)
Eau Claire-2019-03	ECC 7	145	19 (32)	1.60 ± 0.06	14.17 ± 1.94	8.86 ± 1.40
Eau Claire-2019-04	ECC 1	153	23 (31)	1.28 ± 0.05	14.27 ± 1.75	11.17 ± 1.64
Eau Claire-2019-05	ECC 1	242	20 (27)	1.78 ± 0.07	18.01 ± 1.81	10.14 ± 1.30
Eau Claire-2019-06	ECC 1	275	17 (27)	1.40 ± 0.05	15.71 ± 2.02	11.25 ± 1.71

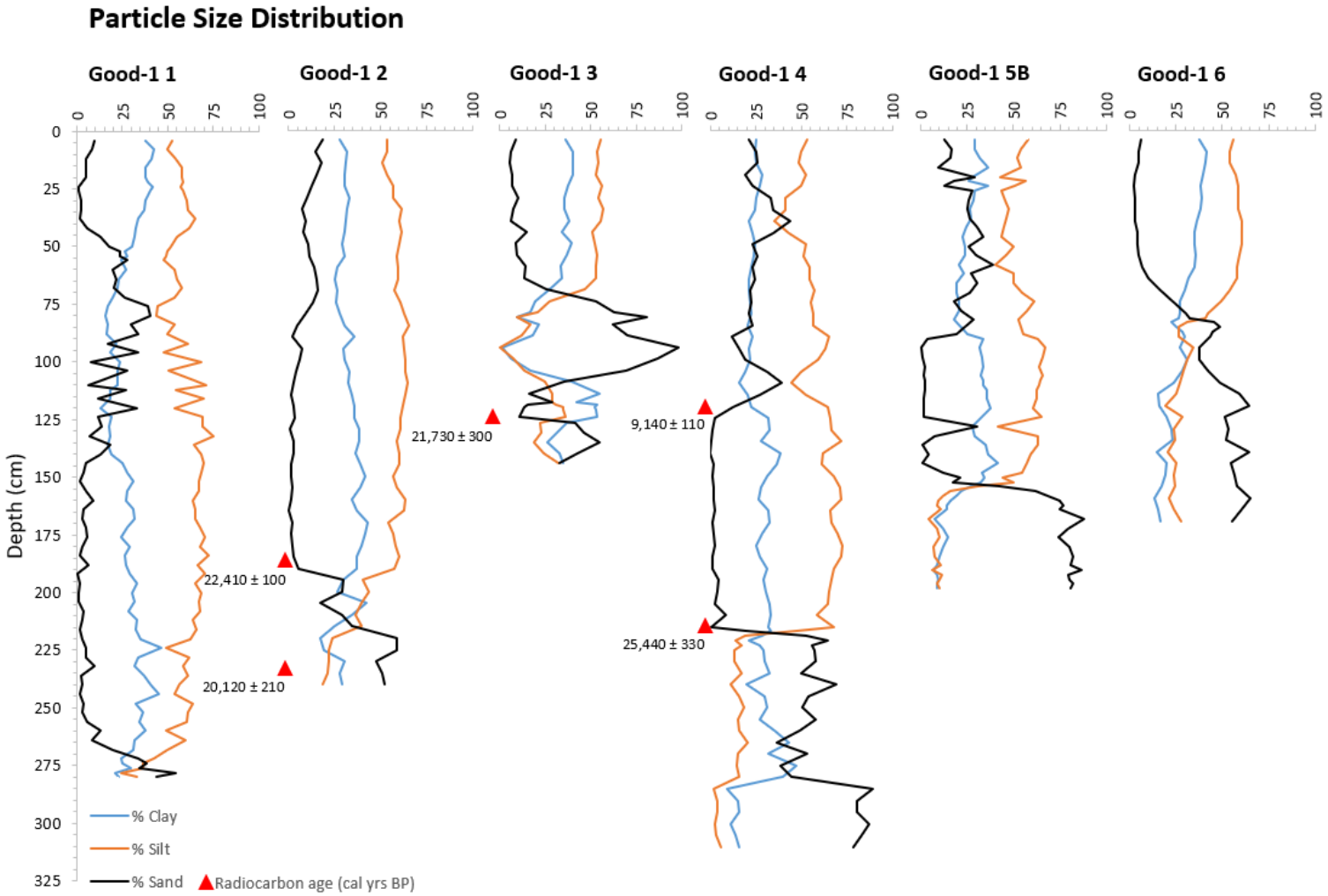

Figure 2.6. Good-1 sand stringer particle size distributions showing percent sand, silt, and clay with depth and radiocarbon ages.

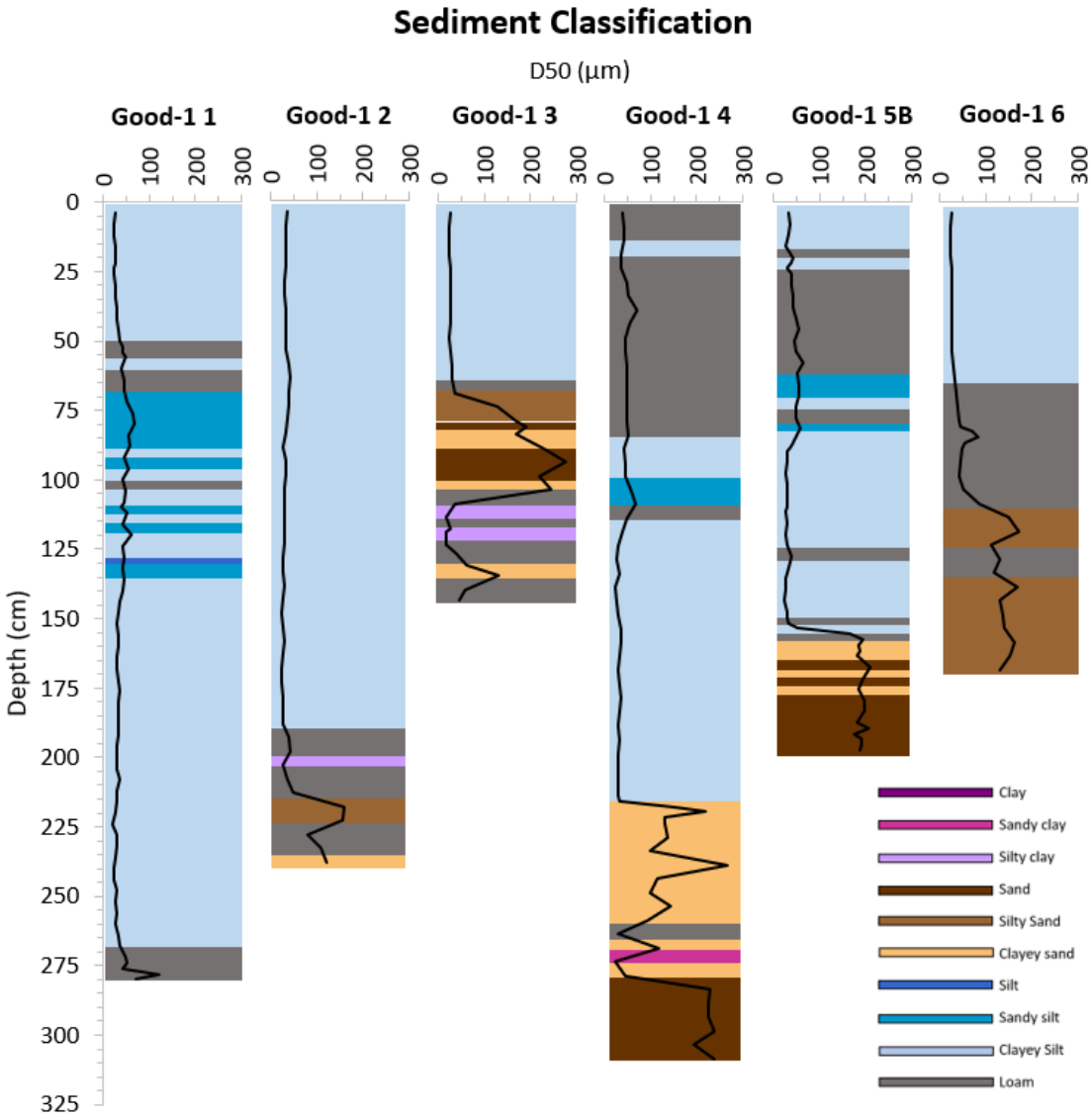

Figure 2.7. Good-1 Shepard sediment classification and median particle size (D50) with depth.

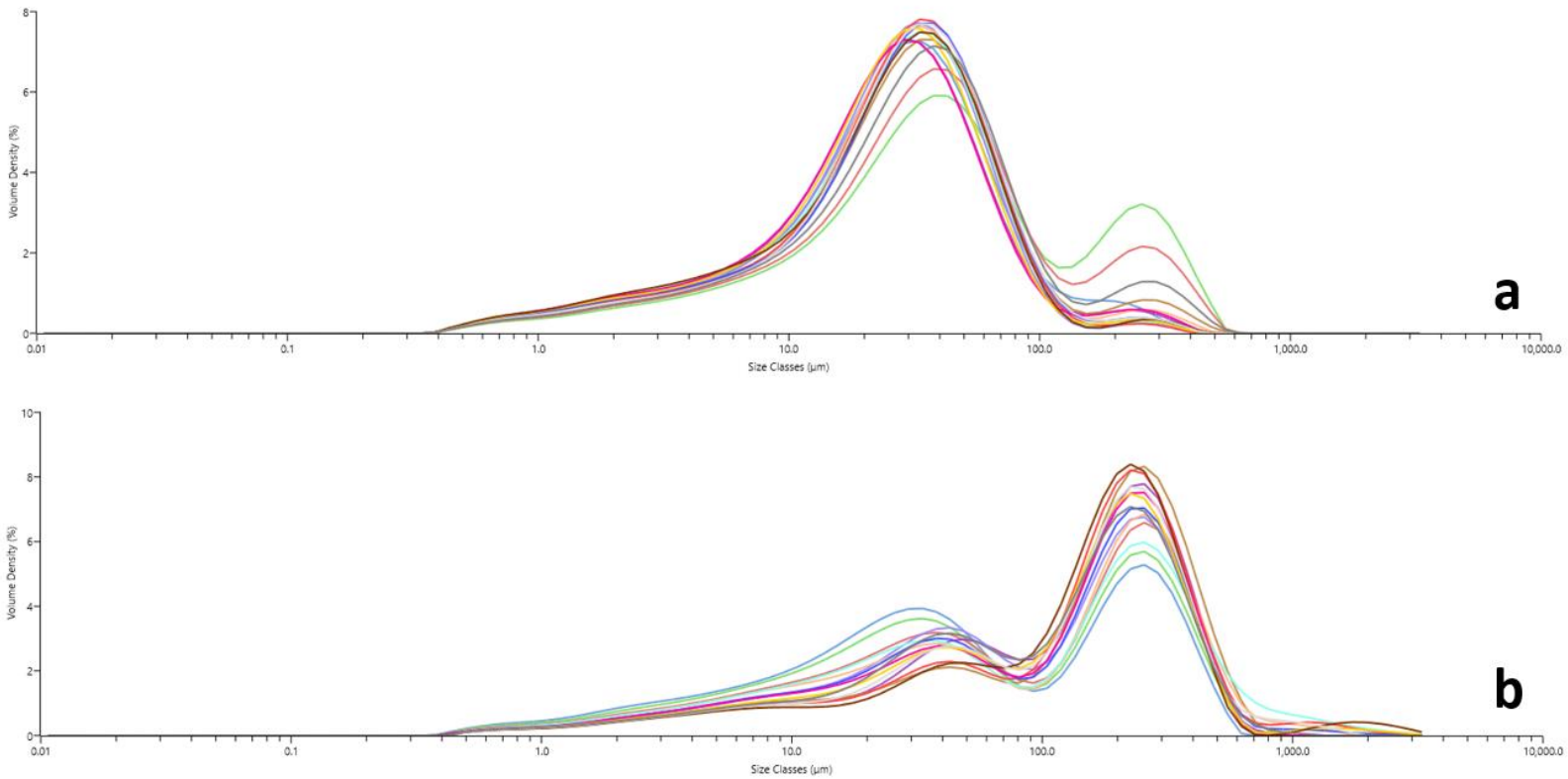

Figure 2.8. Representative grain size distributions from Good-1 core 6. (a) 15 samples from depths 1-84 cm depicting a bimodal distribution for the upper silt-rich unit (Ap, A, B, and BC horizons), and (b) 15 samples from depths 84-172 cm depicting a bimodal distribution for the underlying sand-rich unit (2C horizon).

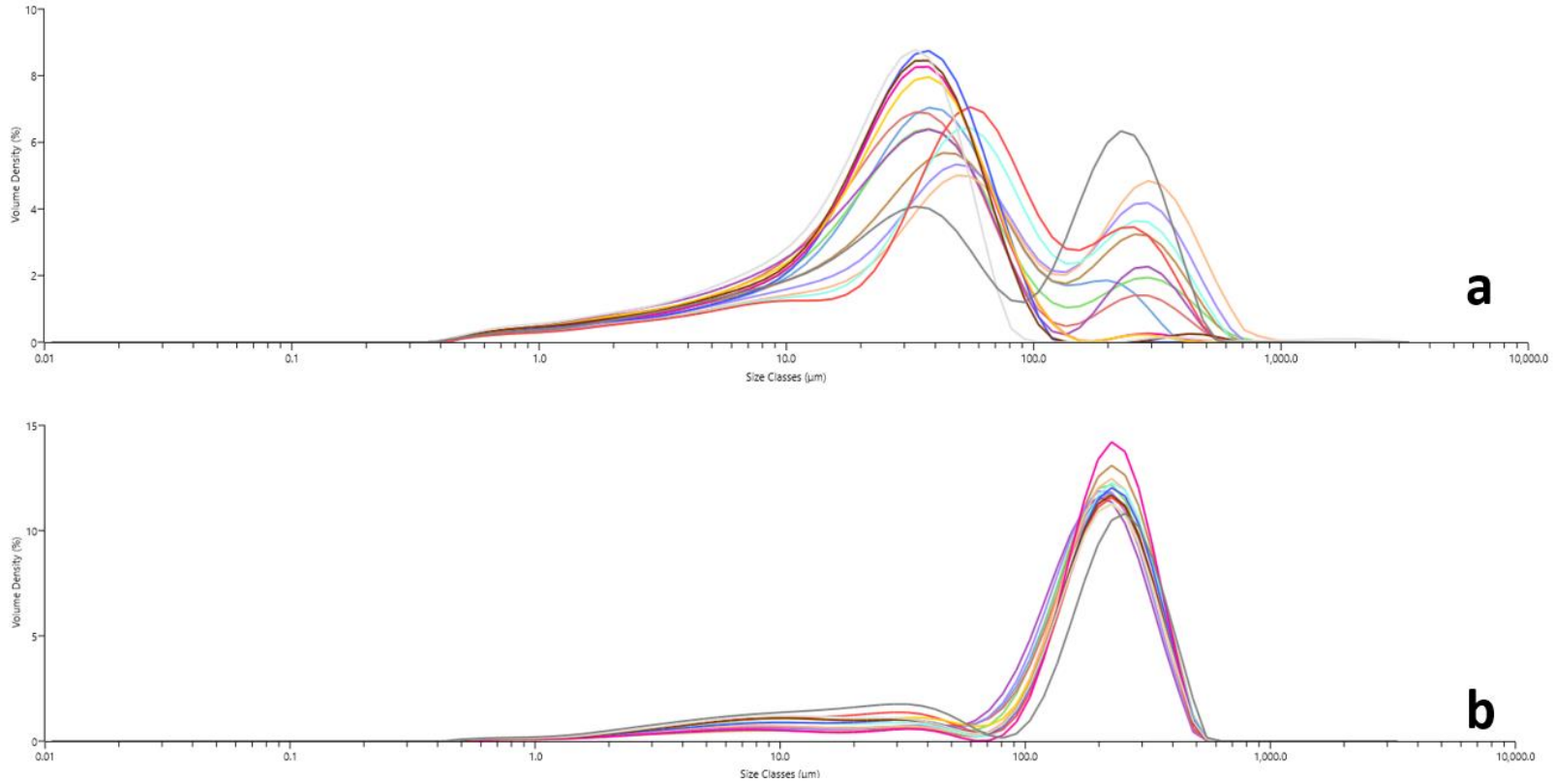

Figure 2.9. Grain size distributions from Good-1 core 5B. (a) 15 samples from depths 1-155 cm in the upper silt-rich unit (Ap, B, C, and C2 horizons), and (b) 15 samples from depths 155-199 cm in the underlying sand-rich unit (2C horizon).

The complex stratigraphy observed within soil cores at ECC was also revealed in the particle size data. The upper 40 cm to 80 cm of most ECC cores corresponds with the Ap, A, AB, B, Bt, BC, and CB horizons and is dominated by silt and clay. Percentages of silt and clay range from ~60-80% on the stringer and ~75-92% on the valley floor (core 3) (Fig. 2.10). This upper unit primarily has a Shepard classification of loam and median grain size ranges from ~21 µm to 82 µm, with USDA particle size classes of coarse silt to very fine sand, respectively (Fig. 2.11). On the valley floor, the upper ~40 cm has a finer texture with a median particle size class bordering coarse to fine silt. In contrast, cores 4 and 7 have a higher sand content than the other ECC cores, with D50 values of ~80 µm to 180 µm (very fine sand to fine sand) and Shepard classification of silty sand. A sample collected at a depth of 61 cm from a 6-cm thick dark brown zone in Core 1 returned a radiocarbon age of 1,320 ± 20 cal yrs BP. Iron masses are common at the base of this unit and typically form the boundary above the underlying stratified sand unit.

Based on particle size distributions, the underlying stratified unit can be subdivided into upper and lower stratified sand units corresponding to the 2C and 3C horizons, respectively. The upper stratified sand unit consists of layers of sand, silty sand, and clayey sand based on Shepard classifications. Iron-cemented layers are common in this unit and have increased silt and clay content and decreased sand content by 20-50%. Throughout this upper sand unit, percentages of sand are highly variable, ranging from ~40-97%, and D50 ranges from ~100 µm to 550 µm. Core 5 differs

slightly, with a lower sand content of 11-69% and D50 ranging from ~30 µm to 300 µm, and only four samples with D50 >100 µm. Samples from this unit returned radiocarbon ages of 6,260 ± 40 cal yrs BP at a depth of 94 cm and 8,000 ± 30 cal yrs BP at a depth of 128 cm from dark brown zones in core 1. A dark brown zone at 91 cm returned an age of only 1,990 ± 50 cal yrs BP in core 7. There is a large discrepancy between radiocarbon ages in this unit, with core 7 producing an age ~4,000 years younger than core 1. This could be due to potential contamination of the sample in core 7 by younger carbon since this sandy unit is highly permeable and within ~50 cm of the rooting zone. It is likely that radiocarbon ages from this unit in core 1 are more accurate due to their relation to other ages gathered at this core. More robust age control is needed at core 7 to better account for this discrepancy. OSL ages from this unit are 11.17 ± 1.64 ka at a depth of 153 cm in core 1 and 8.86 ± 1.40 ka at a depth of 145 cm in core 7 (Table 2.17).

The lower stratified sand unit is denoted in cores 4, 5, 6, and 7 by an increase in sand content, with an increase in percent sand and sharp increase in D50. The shift occurs in core 4 at 194 cm, core 5 at 130 cm, core 6 at 140 cm, and core 7 at 218 cm. Core 5 also has gravels and pebbles present in this unit. A finer-grained basal unit (4C horizon) was also retrieved in cores 4, 6, and 7, the three cores that extend to the greatest depth. Only the top 6-10 cm of this unit were captured in the cores. The basal unit has a median grain size of ~100 µm and Shepard classifications of silty sand, clayey sand, sandy silt, and loam. Two OSL samples adjacent to core 1 were submitted from

depths beyond what was retrieved from the soil cores. The corresponding ages are 10.14 ± 1.30 ka at a depth of 242 cm and 11.25 ± 1.71 ka at 275 cm, and core logs indicate samples were collected from fine sand. The OSL age inversion at 153 cm and 242 cm in core 1 is minimal as both ages are within the margin of error for each other.

Grain size distributions for ECC are highly variable among cores. The Ap, A, AB, B, and Bt horizons exhibit one of three distributions: (1) primary peak from 20-40 μm and secondary peak from 200-300 μm (e.g., cores 1 and 3), (2) primary peak from 100-200 μm and secondary peak from 20-40 μm (e.g., cores 2, 4, and 7), or (3) wide curve from 20-400 μm with a peak ~30 μm (e.g., cores 5 and 6) (Fig. 2.12).

The BC/CB horizons have more complicated grain size distributions. Cores 1 and 2 are similar, having predominantly bimodal distributions with a primary peak of ~100 μm and secondary peak ranging from 20-30 μm. Core 1 has a shift to coarser sediment in the BC2 horizon, with a peak centered around ~300-500 μm. Samples within cores 1 (53-63 cm) and 2 (63-75 cm; 91-97 cm), taken from iron-stained zones, have wider grain size distributions skewed towards fine grains. Grain size distributions for cores 4 and 5 are similar within the BC/CB horizons. Both cores have peaks at ~150 μm and ~100 μm, respectively, that had shoulders around ~300 μm. Both cores have small secondary peaks centered around ~20-30 μm. From 66-82 cm at core 4, there is an increase of fines, but the grain size distribution is similar to other samples from cores 4 and 5. Core 3 is coarser than the other cores in the BC/CB horizons, with a peak around ~300-500

µm and small secondary peak around ~10-30 µm. The CB horizon at core 3 is also somewhat coarser, with a peak around ~100-1000 µm. Most samples from the BC and BC2 horizons from Core 6 have a peak from 20-30 µm and a secondary peak from 300-500 µm, except for samples from an iron-stained zone at 78-81 cm that had a wide distribution. Core 7 has some bimodal samples with nearly equal peaks at ~100 µm and 400-500 µm, but overall sample peaks range from 100-1000 µm with small secondary peaks around ~10-30 µm skewed towards the fines.

The 2C stratified horizons represent the upper stratified sand unit within the cores with all grain size distributions highly variable through the horizon/unit. Cores 1, 2, 3, and 4 are similar. Grain size distributions are generally shifted to the coarser end (>300 µm), with no clear trend within the iron-stained zones (Fig. 2.13a). Core 4 also has samples with distributions that peak between 100 and 200 µm. Most of the peaks in core 5 occur between 40 µm and 200 µm, with secondary peaks at ~400 µm. Cores 6 and 7 have peaks ranging from ~100-700 µm, with no clear trend in the iron-stained zones.

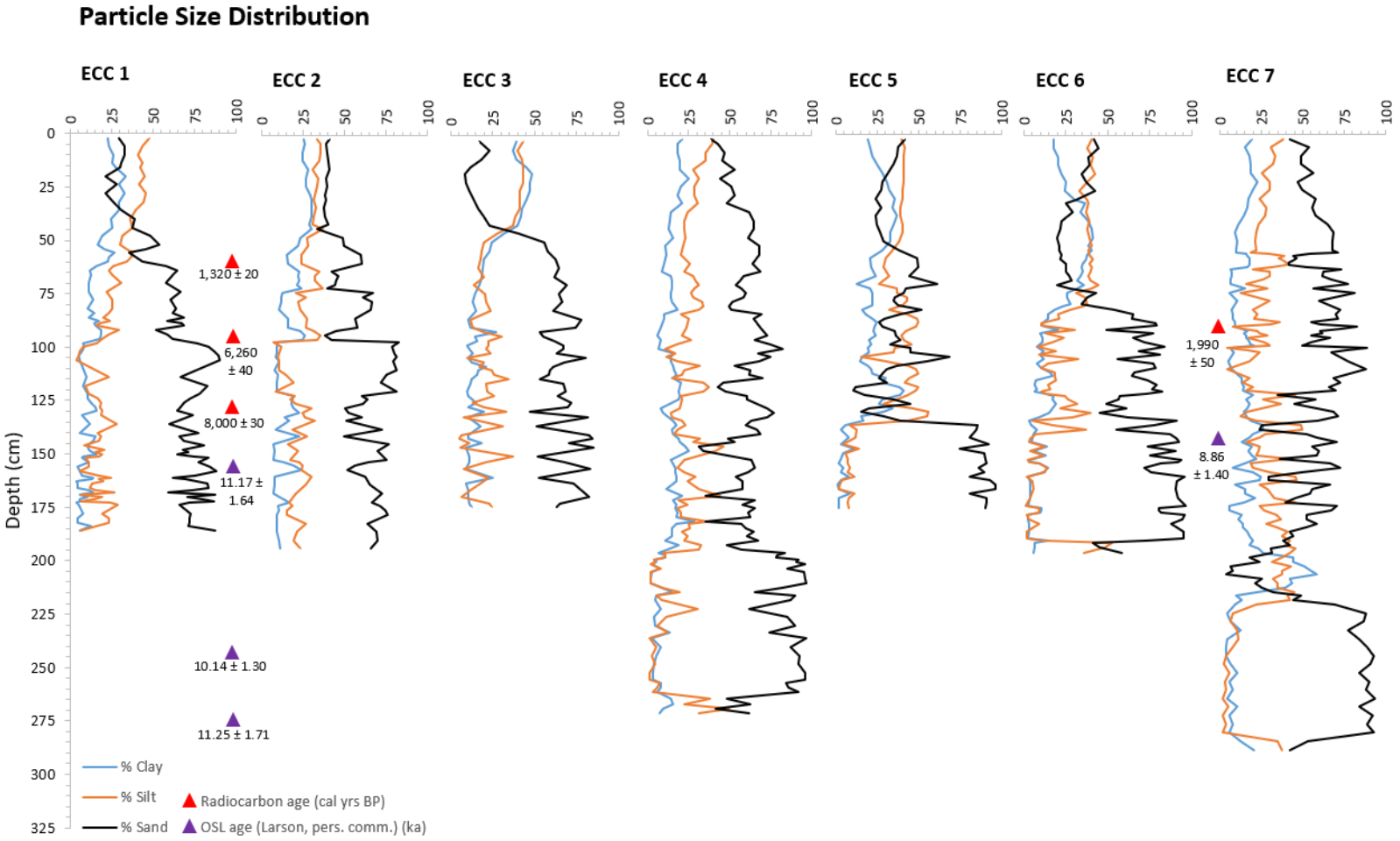

Figure 2.10. ECC particle size distributions showing percent sand, silt, and clay with depth, OSL ages (unpublished ages, Larson, pers. comm.), and radiocarbon ages.

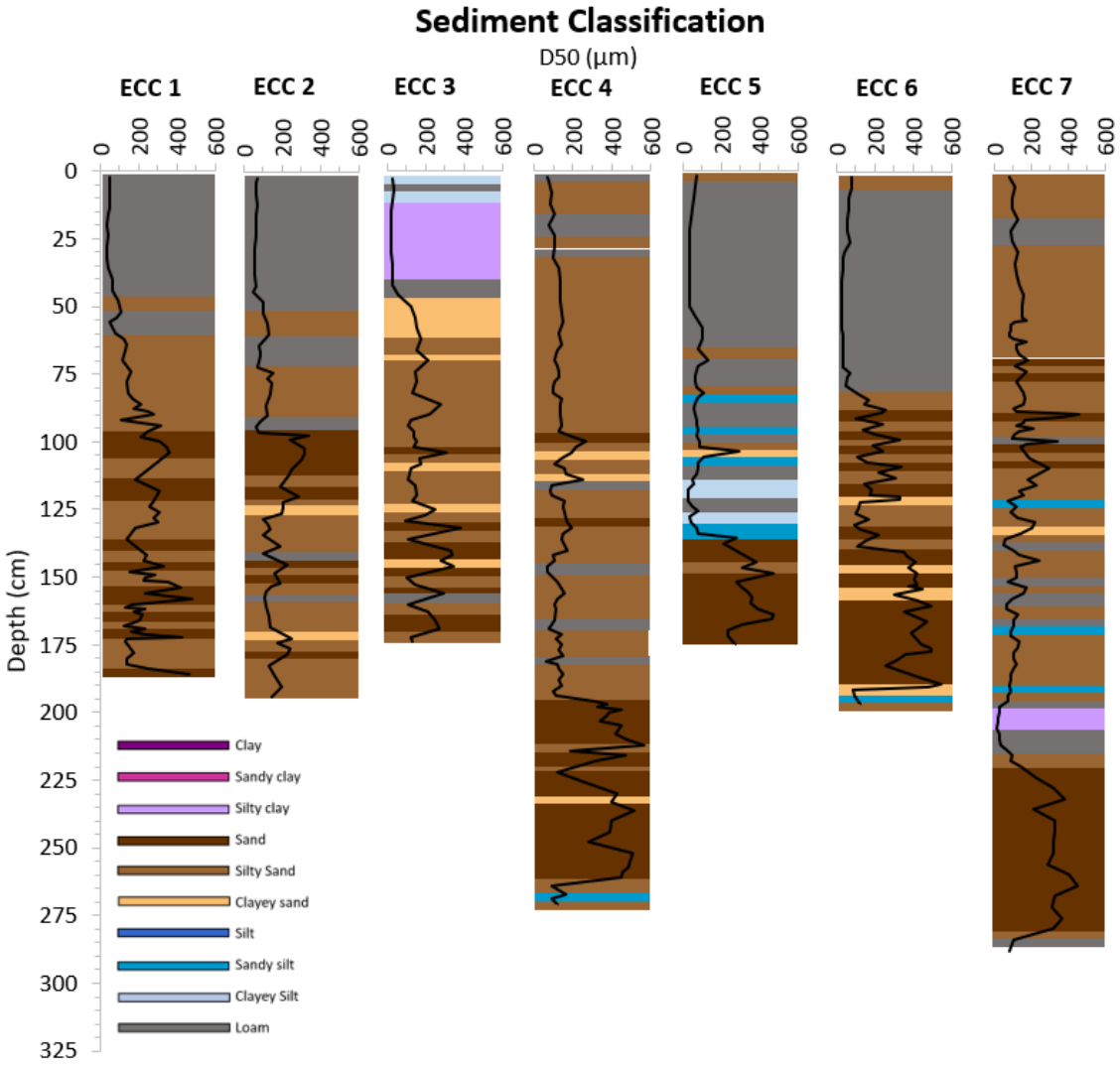

Figure 2.11. ECC Shepard sediment classification and median particle size (D50) with depth.

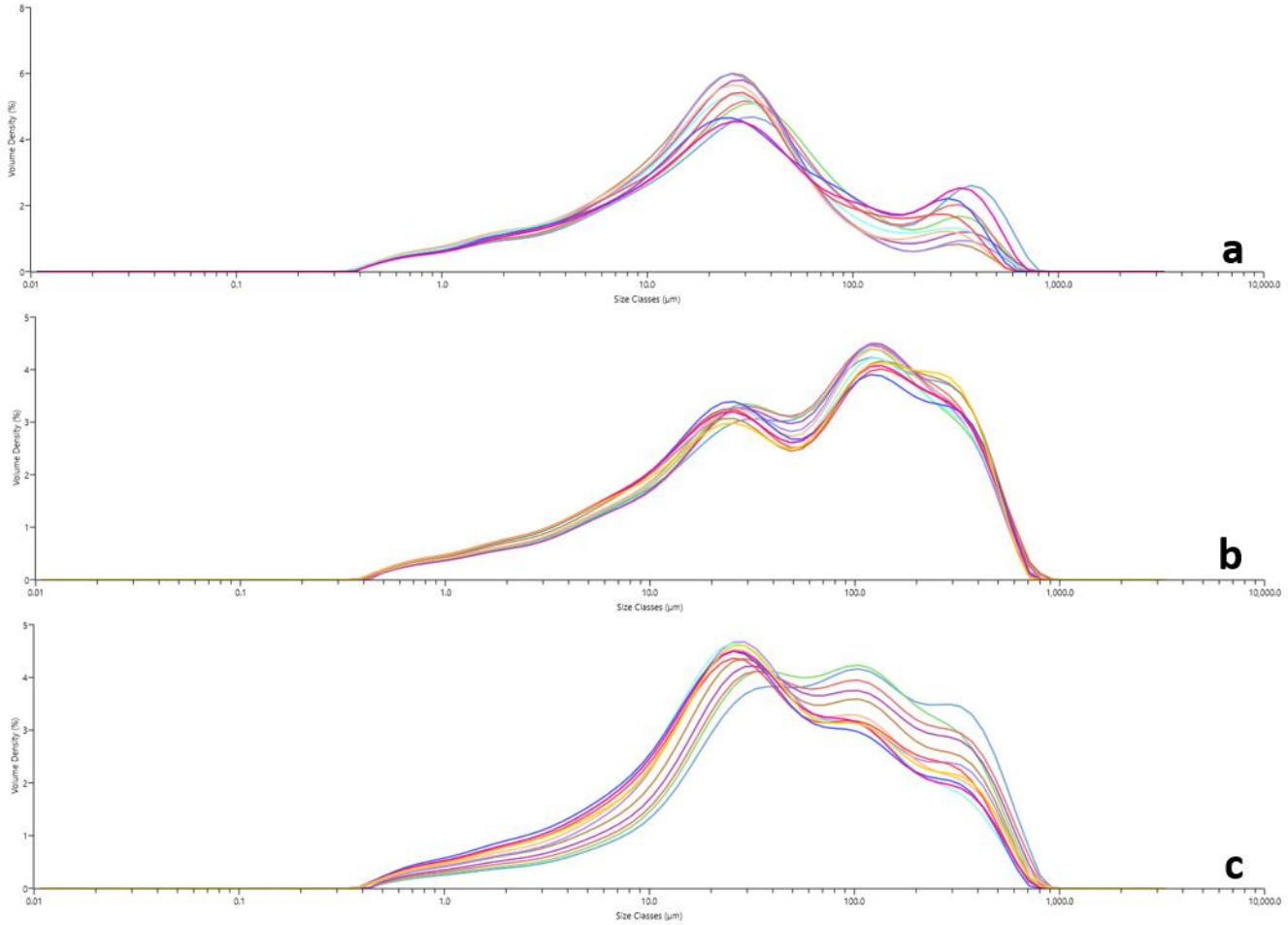

Figure 2.12. Grain size distributions from upper sandy loam unit at ECC. (a) 11 samples from depths 1-47 cm at ECC 3 (A, AB, and Bt horizons), (b) 12 samples from depths of 1-45 cm at ECC 2 (Ap, A, and B horizons), and (c) 12 samples from depths 1-58 cm at ECC 5 (A and Bt horizons).

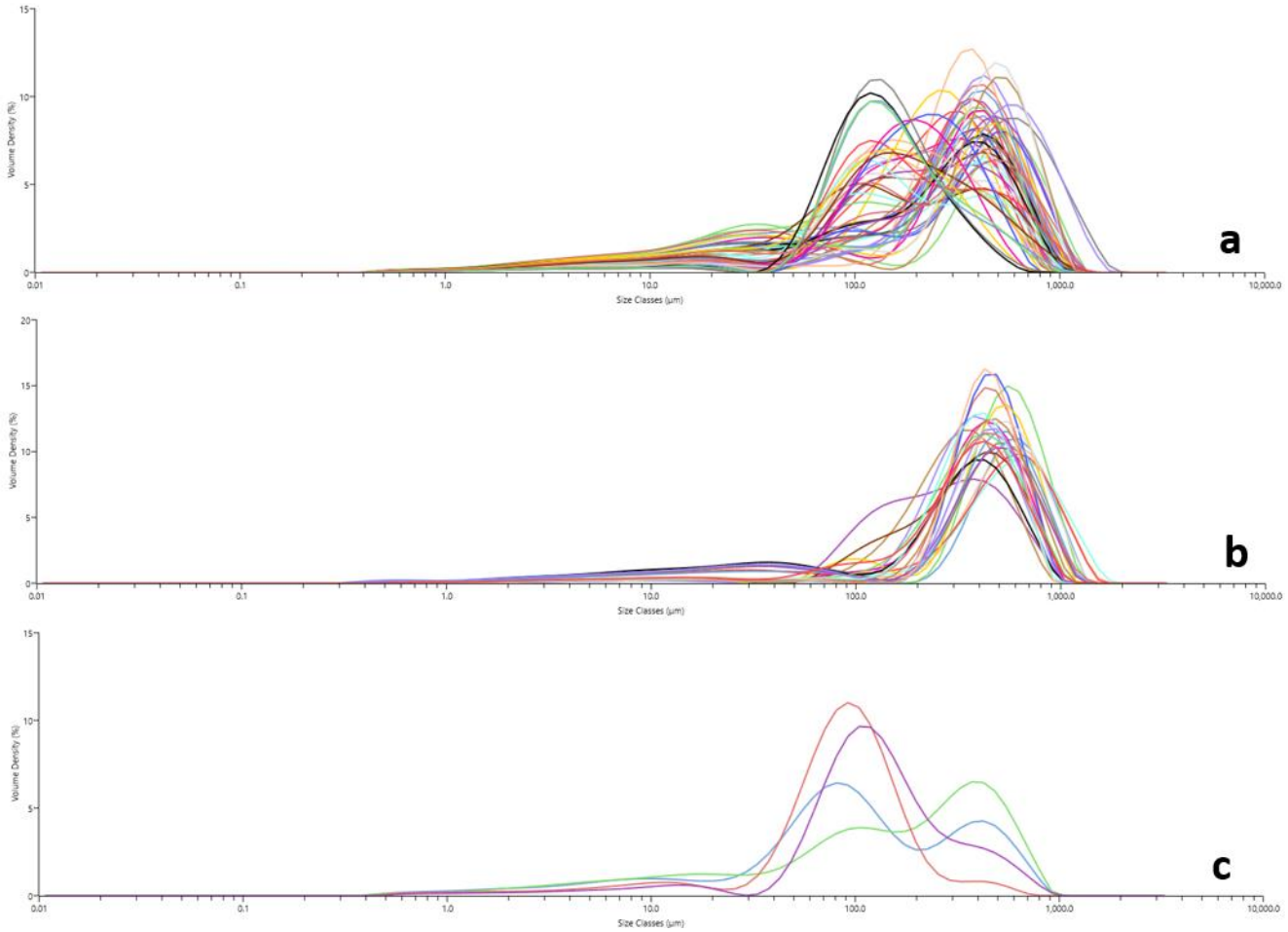

Figure 2.13. Grain size distributions from lower units at ECC. (a) 45 samples from depths of 88-186 cm from the upper stratified unit at ECC 1 (2C horizon), (b) 22 samples from depths of 140-192 cm from the lower stratified unit at ECC 6 (3C horizon), and (c) 4 samples from depths of 264-274 cm from the basal unit at ECC 4 (4C horizon).

The 3C stratified horizons (lower stratified sand unit) were captured in cores 4, 5, 6, and 7. Cores 4, 6, and 7 are similar, showing a shift to the coarser end of the distribution with peaks ~300-600 µm and no clear trend within the iron-stained zones (Fig. 2.13b). Core 7 did have a few samples shifted to finer-grains. Core 5 is highly variable, with peaks from ~80 µm to 600 µm and samples between 142-168 cm peaking between ~300-600 µm. The 4C horizon (basal unit) encountered in cores 4, 6, and 7 is much finer, with a peak at ~100 µm and secondary peak centered around ~300-400 µm (Fig. 2.13c).

2.5. Discussion

2.5.1. Sand Stringer Morphology

Good-1 and ECC have morphologies similar to typical sand stringers described in the literature (Koch and Walters, 2004; Mason et al., 1999; Millett et al., 2018; Schaetzl et al., 2018; Zanner, 1999). Sand stringers have been previously described in the following ways: (1) 3-5 m in height, 20-100 m wide, and up to 20 km in length (Koch and Walters, 2004), (2) 1.5-3 m in height, ~100 m wide, and exceeding 1 km in length (Schaetzl et al., 2018), (3) 1.5-3 m in height, up to 100 m wide, and 10-100s of m in length (Millett et al., 2018), (4) up to 1 m in height, up to 50 m wide, and up to 7 km in length (Zanner, 1999), and (5) 1-3 m in height and several kilometers in length (Mason et al., 1999). In addition to remotely identifying several sand stringers from aerial

imagery, Zanner (1999) also surveyed the Canfield Creek stringer which he determined to be ~2.3 km long.

Previous studies have noted sand stringers are predominantly oriented northwest-southeast (Koch and Walters, 2004; Mason et al., 1999; Millett et al., 2018; Schaetzl et al., 2018; Zanner, 1999). The sand stringers investigated in this study also have a northwest-southeast orientation. Some Midwestern aeolian studies note easterly wind flow off the Laurentide Ice Sheet (COHMAP Members, 1988; Krist and Schaetzl, 2001; Vader et al., 2012), but these sites were directly adjacent to the ice margin. Based upon orientation of Good-1, ECC, and other sand stringers and aeolian landforms within western Wisconsin and southeastern Minnesota, the prevailing wind at the time of sand stringer formation was likely from the west or northwest (Keen and Shane, 1990; Mason et al., 1999; Millett, 2019; Rawling et al., 2008; Schaetzl et al., 2018; Stanley and Schaetzl, 2011; Zanner, 1999). Additionally, Good-1 and ECC are situated on broad, gently sloping valleys open to the west-northwest, further supporting the hypothesis that these landforms are aeolian and were formed due to a predominant west-northwest wind regime. More research is needed to investigate the internal sedimentary structure to test this hypothesis and elucidate the aeolian processes that result in this landform.

2.5.2. Sand Stringer Stratigraphy

Soil core descriptions and particle size analysis at Good-1 reveal three main stratigraphic units: (1) an ~80-270-cm-thick silt-rich upper unit (2) a ~15-100-cm-thick lower sand unit, and (3) a dark brown paleosurface unit found at ~120-220 cm in depth (Fig. 2.4). Based on grain size distributions of the upper silt-rich unit, sediment had a large fine-grained component indicating transport via suspension (Figs. 2.8a and 2.9a), the typical transport mechanism for loess (Sun et al., 2002). This silt-rich unit is interpreted to be Peoria Loess, which is the predominant surficial deposit throughout much of Goodhue county, including surrounding and immediately upwind of the sand stringer (Hobbs and Setterholm, 1998). Peoria Loess was deposited regionally 25-12 ka (Leigh and Knox, 1994), and generally decreases in thickness from west to east (Mason et al., 1994) across southeast Minnesota. The area surrounding Good-1 is mapped as having 1-5-m-thick loess (Muhs et al., 2008). Potential sources for the Peoria Loess unit at Good-1 include sediments from the pre-Wisconsinan Iowan erosion zone or Wisconsinan glacial outwash plains (Mason et al., 1994) near the Des Moines Lobe. Outwash plains seem most likely as the Des Moines Lobe terminal moraine boundary is ~65 km west and the Cannon River that drained the Des Moines Lobe ice (Hobbs and Setterholm, 1998) is ~10 km northwest of Good-1. Conversely, the Iowan erosion zone is primarily southwest of the Good-1 stringer and given the morphology, orientation, and

prior regional aeolian literature, it is likely that west-northwesterly winds were depositing these aeolian sediments.

Most cores from Good-1 have increased sand content within the upper silt unit (Figs. 2.6 and 2.7). Given the coarse sediment size and that Belle Creek, a deeply incised stream with more than 60 m of relief and several prominent bedrock outcrops along its east bank, flows south to north ~4 km west of Good-1, the sand was likely deflated from surrounding outwash and till plains or proximal sandy alluvial deposits. A sample from the B horizon of the upper silt unit returned a radiocarbon age from the Early Holocene (~9 ka), while radiocarbon ages from the base of this unit are Late Pleistocene in age (~22-25 ka) (Table 2.16). Thus, grain size distributions and ages from Good-1 largely correspond with regional Peoria Loess deposition between 25-12 ka (Leigh and Knox, 1994).

The lower sand unit identified at Good-1 is interpreted as glacial outwash and reworked alluvial deposits based upon its coarser grain size (Figs. 2.6 and 2.7) and the inclusion of gravels. The valley floor that Good-1 is situated on is mapped as surficial glaciofluvial and till deposits, and sandy alluvial deposits are mapped within 1 km of Good-1 (Hobbs and Setterholm, 1998). Grain size distributions for this unit indicate a larger coarse fraction (Figs. 5b and 6b), suggesting sediment transport was predominantly from proximal sources (Sun et al., 2002). The sand unit is composed of a

considerable fine-grained fraction, particularly silt, indicating deposition of loess derived from distal sources was also important.

Cores 2 and 3 at Good-1 captured the top of a paleosurface unit which is believed to have existed prior to the deposition of glacial outwash in the study area and sand stringer formation. Surficial geology suggests the paleosurface may be the Pierce Formation, a pre-Wisconsinan glacial till deposit (Hobbs and Setterholm, 1998). However, the top of the paleosurface unit returned radiocarbon ages from the Late Pleistocene during and following the LGM (~22-20 ka) (Table 2.16). Further examination of this unit is required to better understand its age and origin.

ECC has greater sand content and coarser grain size distributions than Good-1 (Figs. 2.12 and 2.13), suggesting sediment was primarily transported via saltation and traction (Sun et al., 2002). Soils surrounding ECC are predominantly mapped as alluvial and aeolian sandy loams and loamy sands (Soil Survey Staff, 2019). ECC cores revealed four distinct stratigraphic units: (1) an ~80-100-cm-thick sandy loam surface unit, (2) a ~60-160-cm-thick upper stratified sand unit, (3) a ~50-70-cm-thick lower stratified sand unit, and (4) a finer grained basal unit found at ~190-280 cm in depth (Fig. 2.5). The sandy loam and upper stratified units are interpreted as the main body of the sand stringer. Radiocarbon data indicate that all or most of this sandy loam unit was deposited within the last 2,000 years (Table 2.16); however, significant discrepancies in radiocarbon ages from the northwest (core 1) and southeast (core 7) portions of the

stringer at equivalent depths prevent more precise time constraints. A radiocarbon age near the top of the upper stratified unit at core 7 returned a Late Holocene age (~2 ka) (Table 2.16), while at core 1 the same unit returned a Middle Holocene age (~6 ka). Additional radiocarbon ages collected above and below this sample in core 1 are in apparent chronological sequence, suggesting the sample from core 7 was potentially contaminated by modern carbon. Further sampling is necessary to resolve this discrepancy. In comparison, the upper stratified sand unit primarily returned OSL ages ranging from Pleistocene-Holocene transition to Middle Holocene (~8.9-11.3 ka) (Table 2.17). Two of the OSL samples were collected from depths greater than that retrieved via soil-coring, but all OSL samples appear to be from the upper stratified unit.

The lower stratified unit is coarser than the upper stratified unit (Figs. 2.10, 2.11, and 2.13) and appears to have been the primary sand source for the stringer body. Although core 3 on the valley floor did not penetrate deep enough to encounter this lower stratified unit, the unit is interpreted as glacial outwash deposits that are the surficial deposits throughout the upland on which ECC sits, and the sand stringer body is primarily composed of reworked outwash sands. Outwash sands are widely distributed throughout the area (Soil Survey Staff, 2019) and form the dominant surficial deposit along the Chippewa River near ECC (Faulkner et al., 2016; Wisconsin DNR, 2011). The finer-grained unit, only captured in cores 4, 6, and 7, could potentially represent a paleosurface that outwash sands were deposited on, or it could be a relatively thick

fine-grained lamination within the lower stratified unit. Coring was not able to penetrate deep enough to capture enough of this unit to determine its stratigraphic significance.

At ECC stringer, several bands of iron staining or iron cementation were observed, primarily within the stratified units. These iron bands, ranging in thickness from less than 1 cm to greater than 10 cm, could potentially be ortsteins or placic horizons, formed via pedogenesis. Ortsteins are >25-mm-thick cemented horizons that consist of spodic material, while placic horizons are iron and organic matter cemented horizons that vary in thickness (Bockheim, 2014; Soil Survey Staff, 2014, 1999). However, iron bands have also been observed at distinct textural boundaries. Shifts in soil texture can cause water to perch, leading to iron reduction, and subsequent drying allows iron to re-oxidize at the textural discontinuity (Bockheim, 2014). Obear et al. (2014) studied iron bands similar to placic horizons in golf courses around the United States and determined iron concentrated at textural discontinuities in less than 10 years. Given the high sand content at ECC and that the sand has relatively low surface area and relatively high percolation rates, couplets of iron eluviation and illuviation can form relatively quickly (Schaetzl and Thompson, 2015). Cores 4, 5, and 7 had distinct zones of iron depletion indicating prolonged saturation, and all ECC cores had distinct zones of iron staining (Tables 2.9-2.15). Several textural changes were also noted throughout the stringer based upon particle size data. Infiltrating water was potentially

getting perched at these lithologic discontinuities, leading to the formation of iron-stained and iron-cemented bands identified throughout the stringer.

2.6. Conclusion

Based on sand stringer morphology, stratigraphy, and chronology, it is likely that Good-1 began forming shortly after the LGM, while ECC formation began around the Pleistocene-Holocene transition. During glacial retreat after the LGM, outwash was deposited across the landscape (Faulkner et al., 2016; Hobbs and Setterholm, 1998; Syverson, 2007). At this time, Peoria Loess was being transported and deposited from the west (Leigh and Knox, 1994), providing a sediment source for Good-1. As permafrost vacated the study area at ~13-12 ka (Clayton et al., 2001; Loope, 2012; Mason, 2015), outwash sands on sparsely vegetated landscapes also became available for aeolian transport via northwesterly winds (Schaetzl et al., Submitted). Outwash sands are the main sediment source for ECC, although increased sand in Good-1 cores suggest reworked outwash sand was deposited at that site as well. Differing sediment sources resulted in unique stratigraphy and grain size distributions between the two sites. Sand stringer evolution presumably continued into the Early Holocene and early Middle Holocene at both sites. Levels of pedogenesis at Good-1 and ECC indicate stabilization during much of the Middle Holocene and Late Holocene. Following stabilization at ECC, water infiltration coupled with high iron content led to the formation of iron-stained and/or iron-cemented bands along textural discontinuities within the sand stringer.

Zanner (1999) has been the only other comprehensive sand stringer study in this region. Canfield Creek stringer exhibits similar morphology, yet different stratigraphy compared to Good-1 and ECC. Differences in stratigraphy among Good-1, ECC, and Canfield Creek highlight the complexity of past aeolian systems in the Upper Midwest and are likely indicative of the varied sediment sources contributing to landforms via aeolian processes. To better understand the formation and evolution of sand stringers, further stratigraphic and sedimentologic studies are needed at additional sites across the region.

CHAPTER 3: HOLOCENE RECORDS OF ENVIRONMENTAL CHANGE IN SAND STRINGERS OF THE UPPER MIDWEST, USA

3.1. Introduction

The Upper Midwest, USA (i.e., Minnesota, Iowa, Illinois, Wisconsin, Michigan) has experienced significant climate fluctuations since the Last Glacial Maximum (LGM) 26.5-19 ka (Clark et al., 2009). Potentially indicative of these climatic changes are periods of aeolian transport and deposition, as noted by the diverse array of aeolian landforms and deposits (e.g., loess, sand ramps, sand sheets, parabolic dunes, sand stringers, etc.) documented across the region (Arbogast et al., 2015; Colgan et al., 2017; Hanson et al., 2015; Rawling et al., 2008; Schaetzl et al., 2018; Zanner, 1999). Aeolian deposits are often important indicators of paleoenvironmental change in a landscape because of specific climatic conditions necessary for aeolian transport (e.g., dry, sparse vegetation) (Muhs and Zárate, 2001; Pye and Tsoar, 2009; Zanner, 1999). As such, the orientation and morphology of aeolian landforms may be used to infer wind direction(s) at the time of deposition or, potentially, reactivation of an aeolian deposit (Muhs and Zárate, 2001; Pye and Tsoar, 2009; Zanner, 1999).

One such landform that is poorly understood in the Upper Midwest are sand stringers. Sand stringers are subtle, linear, aeolian landforms, and are ubiquitous in the Upper Midwest (Koch and Walters, 2004; Marcou et al., 2019; Millett et al., 2018;

Schaetzl et al., 2018; Zanner, 1999). Typically, sand stringers are <10 m in height, <100 m wide, and several hundred meters to a few kilometers in length with a northwest-southeast orientation (Koch and Walters, 2004; Mason et al., 1999; Millett et al., 2018; Schaetzl et al., 2018; Zanner, 1999). Stringer orientation suggests deposition via northwesterly winds (Schaetzl et al., 2018; Zanner, 1999), and this is similar to the orientation of nearby aeolian landforms noted in the literature (Keen and Shane, 1990; Mason et al., 1999; Rawling et al., 2008; Stanley and Schaetzl, 2011).

Although post-LGM aeolian landforms have been widely documented in the region, the chronology and paleoenvironmental significance of aeolian landforms and deposits in the Upper Midwest remain poorly understood (Schaetzl et al., 2018), with paleoenvironmental studies on sand stringers largely nonexistent. Therefore, sand stringers represent an under investigated potential repository of paleoenvironmental data that can provide novel insight into the relationships between paleoclimate and geomorphic processes in this region following the LGM. The aim of this study is to reconstruct regional paleoclimate and characterize sand stringer formation and evolution in response to shifts in environmental conditions by: (1) measuring magnetic susceptibility of sediments within sand stringer to determine periods of increased pedogenesis, (2) analyzing stable carbon isotopes from stringer soils to reconstruct paleovegetation and paleoclimate, and (3) establishing age control via radiocarbon and

optically stimulated luminescence (OSL) dating to determine the spatial and temporal patterns in deposition of aeolian sand stringers in this region.

3.2. Study Area

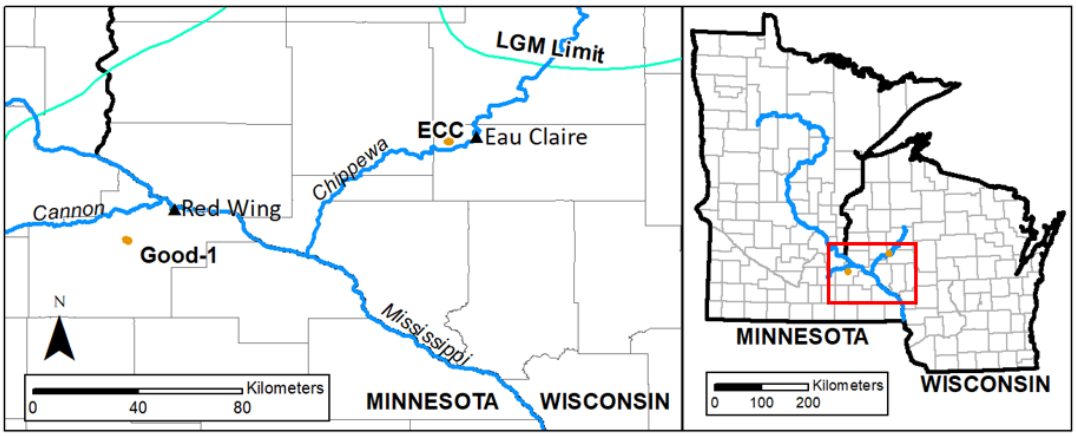

Figure 3.1. Location of Good-1 sand stringer in Goodhue County, Minnesota and ECC sand stringer in Eau Claire County, Wisconsin. LGM glacial ice limit at 18 ka from Dyke et al. (2003).

Sand stringer research sites are located within Goodhue County, Minnesota (Good-1) and Eau Claire County, Wisconsin (ECC) (Figs. 3.1 and 3.2). Both stringers are located in agricultural fields and are proximal to the Mississippi River with Good-1 located ~18 km to the west and ECC located ~60 km to the northeast. Each exhibit sand stringer morphology consistent with descriptions in the prior literature (Koch and Walters, 2004; Mason et al., 1999; Millett et al., 2018; Schaetzl et al., 2018; Zanner, 1999): ~3-5 m of relief, ~850-950 m in length, ~50 m in width, and oriented northwest-southeast. Modern climate in Goodhue and Eau Claire counties is classified as warm

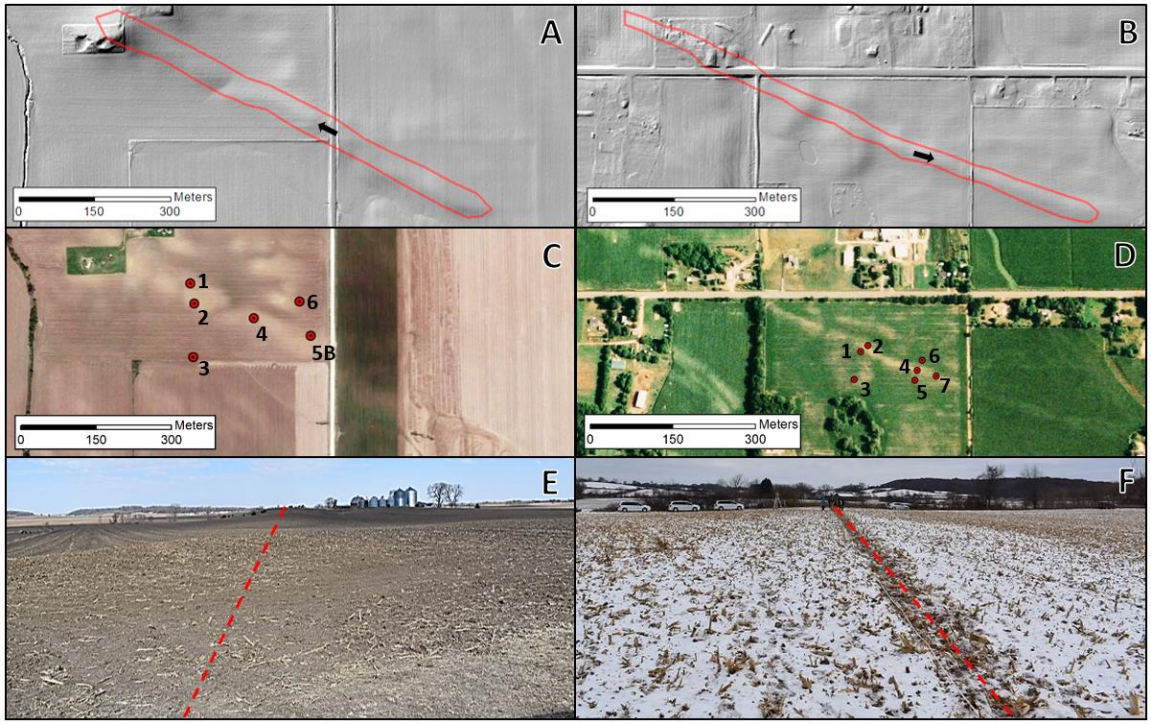

Figure 3.2. (a) Good-1 sand stringer LiDAR digital elevation model (DEM) with hillshade and stringer boundary, (b) ECC sand stringer LiDAR DEM with hillshade and stringer boundary, (c) Good-1 aerial imagery with coring locations, (d) ECC aerial imagery with coring locations, (e) Good-1 ground imagery looking northwest down the crest from the road immediately east of core 5B, and (f) ECC ground imagery looking southeast down the crest from immediately east of core 4.

summer, humid continental (Peel et al., 2007) with an average annual temperature of ~7°C, average annual precipitation of ~78 cm, and average annual snowfall of ~100 cm from 1981-2010 (U.S. Climate Data, 2020a, 2020b). Bedrock geology near Good-1 includes sandstone, dolostone, and sandy dolostone (Runkel, 1998), while bedrock near ECC is sandstone (Brown, 1988), with several outcrops within 2 km of each stringer. Soils within the region are primarily classified as Alfisols, Entisols, and Mollisols (NRCS, 2006).

Good-1 stringer soil is mapped as Mt. Carrol silt loam (Mollic Hapludalf) formed on loess hills (Soil Survey Staff, 2011). ECC stringer soil is mapped as Kevilar sandy loam (Mollic Hapludalf) formed in loamy and sandy alluvium underlain by stratified loamy and sandy alluvium on valley trains (Soil Survey Staff, 2001). Until recently, the soil was classified as Billet sandy loam (Mollic Hapludalf) formed in water- or wind-deposited loamy or sandy sediments (Soil Survey Staff, 2007).

Located within the Driftless Area of Minnesota and Wisconsin, Good-1 and ECC were unglaciated during the LGM (Clayton et al., 2001; Loope, 2012; Mason, 2015). However, periglacial features (e.g., ice and sand wedge casts) suggest permafrost was present in this region until ~12-13 ka (Clayton et al., 2001; Loope, 2012; Mason, 2015; Schaetzl et al., Submitted). Climate at this time was cold and dry (Birks, 1976; Clayton et al., 2001; Muhs and Zárate, 2001; Zanner, 1999), with temperatures in the study area estimated to be as much as 15°C colder than modern (Tierney et al., 2020). Tundra vegetation was dominant across the landscape prior to the Pleistocene-Holocene transition (Birks, 1976; Chumbley et al., 1990; Grigal et al., 1976; Keen and Shane, 1990). A 1-8-m-thick layer of Peoria Loess, which covers much of the bedrock in this region, was deposited during the Late Pleistocene ~25-12 ka (Anderson and Grigal, 1984; Jacobs et al., 1997; Leigh and Knox, 1994; Mason et al., 1994; Muhs and Zárate, 2001; Schaetzl et al., 2018).

Following the LGM, the region experienced a general warming trend through the Middle Holocene (Birks, 1976; Chumbley et al., 1990; Clayton et al., 2001; Grigal et al., 1976; Keen and Shane, 1990; Ma et al., 2004), though there was considerable climatic variability around the Pleistocene-Holocene transition (Nordt et al., 1994). The Bølling-Allerød warm period and the Younger Dryas cold period preceding the Pleistocene-Holocene transition are examples of this variability (Ma et al., 2004). Paleovegetation data is not available proximal to the study areas, so data from central and northern Minnesota and northeastern Iowa have been interpolated. Vegetation shifted from spruce dominated woodlands during the Pleistocene-Holocene transition, to a mixed coniferous-deciduous forest during the Early Holocene (Birks, 1976; Chumbley et al., 1990; Grigal et al., 1976; Keen and Shane, 1990) and to prairie vegetation during the Middle Holocene (Chumbley et al., 1990; Keen and Shane, 1990). During the Late Holocene, an increase in arboreal vegetation suggests decreasing temperature and increasing precipitation at this time (Chumbley et al., 1990; Keen and Shane, 1990).

The morphology of aeolian landforms in the Upper Midwest suggest varied and even conflicting wind regimes since the LGM. According to COHMAP (1988), a strong anticyclone that produced easterly winds was present along the southern edge of the Laurentide Ice Sheet (LIS). This easterly wind regime has been confirmed by various aeolian studies (e.g., Krist and Schaetzl, 2001; Vader et al., 2012). Other studies

have shown, however, that winds during that same period were predominantly from the west and northwest (Arbogast et al., 2015; Colgan et al., 2017; Rawling et al., 2008; Schaetzl et al., 2018; Zanner, 1999).

3.3. Methods

A suite of paleoenvironmental proxies and geochronological dating methods were applied to the soils and sediments within Good-1 and ECC sand stringers. To obtain samples for analysis, a Giddings hydraulic soil coring machine was used to collect six soil-sediment cores from Good-1 and seven soil-sediment cores from ECC in 2.5-cm-diameter, clear, plastic liners (Figs. 3.2c and 3.2d). Core depths ranged from 145 cm to 313 cm at Good-1 and from 177 cm to 289 cm at ECC (Tables 3.1 and 3.2). Cores were sealed and transported to the EARTH Systems Laboratory at Minnesota State University, Mankato for soil profile descriptions and analysis. Elevations for each coring location were determined using LiDAR digital elevation model data and the “Spatial Analyst Extension” and the “Zonal Statistics” tool in ArcMap 10.7.1.

Volumetric and mass-dependent magnetic susceptibility were measured using a Bartington MS3 meter. Volumetric susceptibility was measured in 1-cm-intervals for all thirteen Good-1 and ECC cores using a Bartington MS2C core sensor. It has been suggested that a low measurement interval (i.e., <3-5 cm) can result in an overly smoothed line (Dearing, 1999). To determine an optimal measurement interval, three

cores were analyzed in 1-cm, 2-cm, and 4-cm intervals. Values for the three measurement intervals were nearly identical, with the 1-cm interval providing the highest resolution data. Each core was measured for volumetric susceptibility while the core liner was sealed, and the core was intact. Measurements for the upper and lower 4 cm of each core segment were discarded due to potential dilution effects at the ends of cores (Dearing, 1999).

Table 3.3. Good-1 soil-sediment core information.

Good-1	Elevation (m)	Sand Stringer Geomorphic Position	Core Depth (cm)
1	313.55	South-east facing nose slope	282
2	312.16	Shoulder	241
3	310.06	Valley floor	145
4	313.25	Northwest-facing nose slope/swale	313
5B	317.79	Crest	199
6	316.43	Secondary peak	172

Table 3.4. ECC soil-sediment core information.

ECC	Elevation (m)	Sand Stringer Geomorphic Position	Core Depth (cm)
1	271.70	Crest	186
2	271.60	Shoulder	197
3	271.50	Valley floor	177
4	272.86	Crest	274
5	273.00	Shoulder	177
6	272.90	Shoulder	198
7	273.83	Crest	289

Mass-dependent susceptibility was measured for four cores at Good-1 and four cores at ECC using a Bartington MS2B dual frequency bucket sensor. Core liners were cut open and soil core faces were scraped clean to avoid contamination. Samples for mass-dependent susceptibility were collected in 4-6 cm intervals in 10 cm^3 plastic cubes, dried, and capped before being analyzed in the bucket sensor. Magnetic susceptibility within soils can be enhanced due to a variety of factors, including changes in sediment sources, increased precipitation, or pedogenesis (Evans and Heller, 2003; Maher, 1998). Determining sediment source aids in the understanding of sand stringer formation while rates of pedogenesis are correlated to changes in climate.

Samples for stable carbon isotope analysis were collected in 2-10 cm intervals, adjusting for stratigraphic complexity, from ECC cores 1 and 7, and from Good-1 cores 2 and 4. Samples were dried and ground with visible roots and debris removed before being sealed in sterile whirl-paks and submitted to the W. M. Keck Paleoenvironmental and Environmental Stable Isotope Laboratory (KPESIL) at the University of Kansas. Stable carbon isotope data were used to reconstruct paleovegetation and paleoclimate through fluctuations in C3 and C4 plant contributions to soil organic carbon (SOC) preserved within cores. C3 plants are typically dominant in cool, moist climates while C4 plants are typically dominant in warm, dry climates (Ehleringer and Cerling, 2002). Mean July temperature is the best predictor of C3 versus C4 dominance, with C3 plants dominating when mean July temperature is below 21-22°C, C4 plants dominating above

22°C, and mixed C3-C4 plants between 21-22°C (von Fischer et al., 2008). To estimate the amount of SOC contributed by C3 and C4 plants, the following equation was used (Nordt et al., 1994):

$$\%C4\ biomass = ((\delta^{13}C_{SOC} - \delta^{13}C_{C3}) / (\delta^{13}C_{C4} - \delta^{13}C_{C3})) \times 100$$

where $\delta^{13}C_{SOC}$ is the $\delta^{13}C$ value of SOC relative to the Pee Dee belemnite (PDB) standard, $\delta^{13}C_{C3}$ is the mean value for C3 plants (-27‰), and the $\delta^{13}C_{C4}$ is the mean value for C4 plants (-13‰).

To better understand spatial and temporal variability in sand stringer formation and evolution, age control was established via AMS radiocarbon dating and optically stimulated luminescence (OSL) dating. These geochronological methods were selected because sand stringers contain organic-rich horizons and sand-rich horizons making them suitable for radiocarbon and OSL dating, respectively (Goble et al., 2004). Samples for AMS radiocarbon analysis were collected from Good-1 cores 2, 3, and 4 at depths ranging from 118-235 cm and from ECC cores 1 and 7 at depths ranging from 61-128 cm. Samples were dried and ground with visible roots and debris removed before being sealed in plastic vials and submitted to the National Ocean Sciences Accelerator Mass Spectrometry Lab (NOSAMS) for analysis. Reported radiocarbon ages were converted to calendar ages using the online CALIB 8.2 Radiocarbon Calibration Program (Stuiver et al., 2021). Age control at ECC was also obtained via OSL dating. Three OSL samples adjacent

to core 1 and one OSL sample adjacent to core 7 were collected via bucket augering in opaque metal tubes at depths ranging from 145-275 cm and submitted to the Utah State Luminescence Laboratory. Ages were acquired following the single-aliquot regenerative dose (SAR) method (Murray and Wintle, 2000).

3.4. Results

3.4.1. Sand Stringer Stratigraphy

Based on soil core descriptions, Good-1 stringer has three main stratigraphic units (Table 3.3). The upper unit is silt-rich, ~150-270-cm-thick, and encompasses the majority of Good-1 cores. Soil horizons within this unit include Ap, A, AB, B, BC, and C horizons. This unit returned a radiocarbon age of 9,140 ± 110 cal yrs BP at a depth of 118 cm in core 4, and the base of this silt-rich unit returned ages of 25,440 ± 330 cal yrs BP at 216 cm in core 4 and 22,410 ± 100 cal yrs BP at 188 cm in core 2 (Table 3.5).

Below the silt-rich unit at Good-1 is a >15-100-cm-thick sand unit consisting of the 2C horizon. Cores 2 and 3 captured the upper 0.25 m of a basal unit underlying the sand unit, labeled as the 3C horizon. This basal unit is darker and has a finer texture than the overlying sand unit and is interpreted as a paleosurface that predates stringer formation. Radiocarbon samples taken from the top of the paleosurface unit returned ages of 21,730 ± 300 cal yrs BP at 122 cm in core 3 and 20,120 ± 210 cal yrs BP at 235 cm in core 2. There is an age discrepancy between samples at 188 cm and 235 cm at core 2,

suggesting potential contamination by younger carbon due to natural carbon cycling (Wang et al., 1996).

ECC stringer is more complex and reveals four main stratigraphic units (Table 3.4). The surface unit is a ~60-100-cm-thick sandy loam and is composed of Ap, A, B, Bt, BC, and CB horizons. A radiocarbon sample from a depth of 61 cm in the BC horizon at core 1 returned an age of 1,320 ± 20 cal yrs BP.

Below the surface unit at ECC is a 60-160-cm-thick stratified zone consisting of alternating 1-8-cm-thick iron-stained/iron-cemented sand and structureless sand beds. This stratified zone is divided into an upper and lower unit based on increased sand content in the lower unit. The upper stratified unit consists of the 2C horizon and returned OSL ages of 11.17 ± 1.64 ka at a depth of 153 cm in core 1 and 8.86 ± 1.40 ka at a depth of 145 cm in core 7 (Table 3.6). Radiocarbon samples from this unit returned ages of 6,260 ± 40 cal yrs BP at a depth of 94 cm and 8,000 ± 30 cal yrs BP at a depth of 128 cm at core 1, and 1,990 ± 50 cal yrs BP at a depth of 91 cm at core 7. A large age discrepancy exists between radiocarbon ages within this unit at cores 1 and 7. Ages from core 1 are assumed to be more accurate as more robust age control exists. The young age produced by core 7 is interpreted as being contaminated by younger carbon, but further age control is necessary to better understand this discrepancy.

*Table 3.3. Soil stratigraphy of Good-1. (*stratified horizon)*

Good-1 1		Good-1 2		Good-1 3		Good-1 4		Good-1 5B		Good-1 6	
Depth (cm)	**Soil Horizon**	**Depth (cm)**	**Soil Horizon**	**Depth (cm)**	**Soil Horizon**	**Depth (cm)**	**Soil Horizon**	**Depth (cm)**	**Soil Horizon**	**Depth (cm)**	**Soil Horizon**
0-15	Ap	0-15	Ap	0-16	Ap	0-15	Ap	0-20	Ap	0-16	Ap
15-29	A	15-29	A	16-46	A	15-26	A	20-58	B	16-36	A
29-49	B	29-49	B	46-64	AB	26-55	B	58-85	C	36-54	B
49-71	BC	49-79	BC	64-80	2B	55-116	C	85-155	C2	54-84	BC
71-142	C strat*	79-165	C	80-101	2C	116-214	C2	155-199	2C	84-172	2C
142-267	C2	165-190	C2	101-111	2C2	214-233	2C				
267-276	2C	190-216	2C	111-120	2C3	233-283	2Ck				
276-282	2C2	216-241	3C	120-145	3C	283-313	2C2				

*Table 3.4. Soil stratigraphy of ECC. (*stratified horizon) (**krotovina)*

ECC 1		ECC 2		ECC 3		ECC 4	
Depth (cm)	**Soil Horizon**	**Depth (cm)**	**Soil Horizon**	**Depth (cm)**	**Soil Horizon**	**Depth (cm)**	**Soil Horizon**
0-16	Ap	0-14	Ap	0-13	Ap	0-15	Ap
16-32	Bt	14-24	A	13-20	AB	15-36	B
32-41	Krot**	24-45	B	20-47	Bt	36-84	BC
41-63	BC	45-97	BC	47-59	BC	84-194	2C strat*
63-88	BC2	97-197	2C strat*	59-91	CB	194-264	3C strat*
88-186	2C strat*			91-177	2C strat*	264-274	4C

ECC 5		ECC 6		ECC 7	
Depth (cm)	**Soil Horizon**	**Depth (cm)**	**Soil Horizon**	**Depth (cm)**	**Soil Horizon**
0-16	Ap	0-14	Ap	0-16	Ap
16-58	Bt	14-40	B	16-34	B
58-71	BC	40-57	BC	34-63	BC
71-130	2C strat*	57-81	BC2	63-112	2C strat*
130-177	3C strat*	81-140	2C strat*	112-218	2C2 strat*
		140-192	3C strat*	218-280	3C strat*
		192-198	4C	280-289	4C

*Table 3.5. Radiocarbon ages for Good-1 and ECC. Calendar ages calibrated using the online CALIB 8.2 Radiocarbon Calibration Program; ages rounded to the nearest decade. (*stratified horizon)*

Core Name	Depth (cm)	Soil Horizon	Lab Number	$\delta^{13}C$ (‰)	^{14}C age (yr BP ± 1σ)	Calendar age (yr BP ± 1σ)
ECC 1	61	BC	OS-159317	-21.30	1,410 ± 20	1,320 ± 20
ECC 7	91	2C strat*	OS-157918	-18.95	2,050 ± 20	1,990 ± 50
ECC 1	94	2C strat*	OS-157917	-19.84	5,470 ± 30	6,260 ± 40
ECC 1	128	2C strat*	OS-159383	-22.39	7,210 ± 35	8000 ± 30
Good-1 4	118	C2	OS-159319	-23.13	8,190 ± 30	9,140 ± 110
Good-1 3	122	3C	OS-158458	-19.92	17,900 ± 210	21,730 ± 300
Good-1 2	188	C2	OS-159318	-23.87	18,500 ± 110	22,410 ± 100
Good-1 4	216	2C	OS-158459	-24.31	21,100 ± 310	25,440 ± 330
Good-1 2	235	3C	OS-157919	-19.48	16,650 ± 160	20,120 ± 210

Table 3.6. OSL ages for ECC (Unpublished ages, Larson, pers. comm.)

Core Name (Larson, pers. comm.)	Core Name Equivalent	Depth (cm)	Num. of Aliqouts	Dose rate (Gy/ka)	Equivalent Dose ± 2σ (Gy)	OSL Age ± 2σ (ka)
Eau Claire-2019-03	ECC 7	145	19 (32)	1.60 ± 0.06	14.17 ± 1.94	8.86 ± 1.40
Eau Claire-2019-04	ECC 1	153	23 (31)	1.28 ± 0.05	14.27 ± 1.75	11.17 ± 1.64
Eau Claire-2019-05	ECC 1	242	20 (27)	1.78 ± 0.07	18.01 ± 1.81	10.14 ± 1.30
Eau Claire-2019-06	ECC 1	275	17 (27)	1.40 ± 0.05	15.71 ± 2.02	11.25 ± 1.71

The lower stratified unit, which is coarser in texture, is the 3C horizon retrieved only at cores 4, 5, 6, and 7. The basal unit at ECC is the 4C horizon and only 6-10 cm was captured in cores 4, 6, and 7, the three cores that extended the deepest. This basal unit has a darker color and sharp increase in silt and has been interpreted to be a paleosurface. OSL samples collected from the lower stratified unit adjacent to core 1 returned ages of 10.14 ± 1.30 ka at a depth of 242 cm and 11.25 ± 1.71 ka at 275 cm. There is an age discrepancy between 153 cm and 242 cm in core 1, but the two ages are within the margin of error of each other.

3.4.2. Magnetic Susceptibility

3.4.2.1. Good-1

At Good-1, volumetric susceptibility (κ) was measured for all six cores, while mass-dependent susceptibility (χ) was measured for cores 1, 2, 4, and 5B (Fig. 3.3). Magnetic susceptibility values are greatest in the upper silt-rich unit, which has been modified via pedogenesis. Susceptibility values decrease sharply at the boundary with the underlying sand unit and remain relatively low in most cores.

In core 1, volumetric and mass-dependent magnetic susceptibility of the upper silt-rich unit are relatively uniform with depth, primarily oscillating from ~95-125 κ and ~65-95 χ (m^3/kg) in 10-30 cm intervals, and then declining rapidly within the sand-rich unit (2C horizons) (Fig. 3.3). Core 2 has a similar trend, though values are less oscillatory.

In cores 4 and 5, magnetic susceptibility is enhanced within the Ap-A horizons, declines within the B horizons, and increases within the C and C2 horizons, with values in the C horizons exceeding the Ap-A horizons; magnetic susceptibility declines to near 0 in the 2C horizons. Core 6, collected on a secondary peak adjacent to the main stringer body, has greatest volumetric magnetic susceptibility within the Ap-A horizons, declines through the B and BC horizons, and then becomes highly oscillatory, ranging from ~60-130 κ, within the 2C horizon. On the valley floor (core 3), magnetic susceptibility is enhanced within the Ap-A horizon and exhibits a declining trend with depth, with a peak in the 2B horizon, and low values in the 2C and 3C horizons. Thus, in Good-1 the upper silt-rich unit (Ap-A-B-BC-C horizons) has relatively high magnetic susceptibility, while the underlying sand-rich unit (2C and 2Ck horizons) and paleosurface (3C horizon identified in cores 2 and 3) have low magnetic susceptibility.

Volumetric and mass-dependent susceptibilities generally display similar trends for all Good-1 cores, with one notable discrepancy. At core 5B between ~120-160 cm, mass-dependent susceptibility is much lower than volumetric susceptibility. This unit has a pronounced decrease in sand content, and volumetric susceptibility may be affected by increased bulk density (Dearing, 1999).

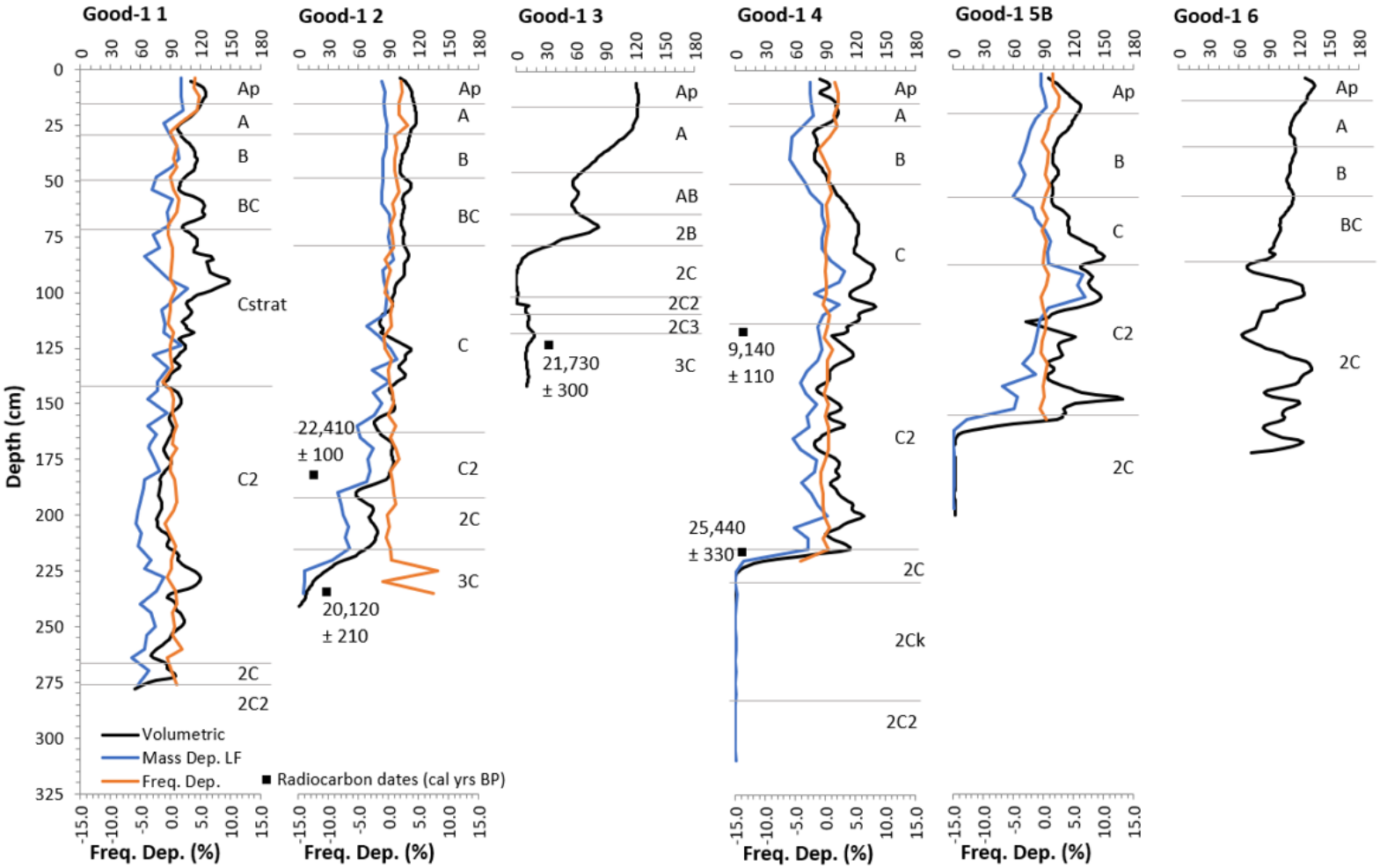

Figure 3.3. Volumetric and frequency dependent magnetic susceptibility and radiocarbon ages for Good-1.

Percent frequency dependence can indicate the influence of pedogenesis based on the presence of superparamagnetic (SP) grains, with values <2% corresponding to low SP grain presence and lack of pedogenesis, 2-10% corresponding to medium SP grain presence and moderate pedogenesis, and >10% corresponding to high SP grain presence and strong influence of pedogenesis (Dearing, 1999). At Good-1, percent frequency dependence generally fluctuates around 0%, suggesting little magnetic enhancement due to pedogenesis. Values are slightly elevated in the upper ~20 cm, with frequency dependences of 3.9-4.9%, 1.8-3.2%, 1.3-2.1%, and 1.5-2.6% in cores 1, 2, 4, and 5B, respectively. Below ~20 cm, frequency dependence decreases below 2% for the remainder of the cores except for core 2, which has two peaks of 8.1% at 225 cm and 7.5% at 235 cm. These peaks are likely erroneous based upon the low susceptibility values found via volumetric and mass-dependent analysis. Frequency dependence was not calculated for the bottom 90 cm of core 4, and bottom 40 cm at core 5B for this reason.

3.4.2.2. ECC

At ECC, volumetric susceptibility was measured for all seven cores, while mass-dependent susceptibility was measured for cores 1, 2, 3, and 7 (Fig. 3.4). Magnetic susceptibility values are enhanced within the surface unit modified by pedogenesis and exhibit a slight declining trend with depth. In the underlying stratified sand units that form the bulk of the stringer, values oscillate with several pronounced peaks.

Volumetric and mass-dependent susceptibility have similar trends throughout all cores, with only minor variations between the two.

The upper sandy loam unit has volumetric magnetic susceptibility values between 70-90 κ and mass-dependent magnetic susceptibility between 50-70 χ (m^3/kg) in the Ap-A horizons, with slight enhancement in the B horizons in all cores. Volumetric and mass-dependent magnetic susceptibility decline slightly through the C horizon. All cores become highly oscillatory in the upper and lower stratified sand units. Volumetric susceptibility oscillates by ~10-20 κ in ~2-10-cm-thick intervals, while mass-dependent susceptibility was measured at too coarse a resolution to identify most oscillations. Peaks in susceptibility values correlate with bands of iron-cemented sand and declines correlate with loose, structureless sand. Extremely high peaks of susceptibility were noted in core 5 at ~160 cm and core 7 at ~225 cm within the 3C horizon. In examining the cores, the cause of these pronounced peaks is unclear. It may be due to fine particles of iron-manganese nodules or iron-oxides, since redoximorphic features are common within these cores.

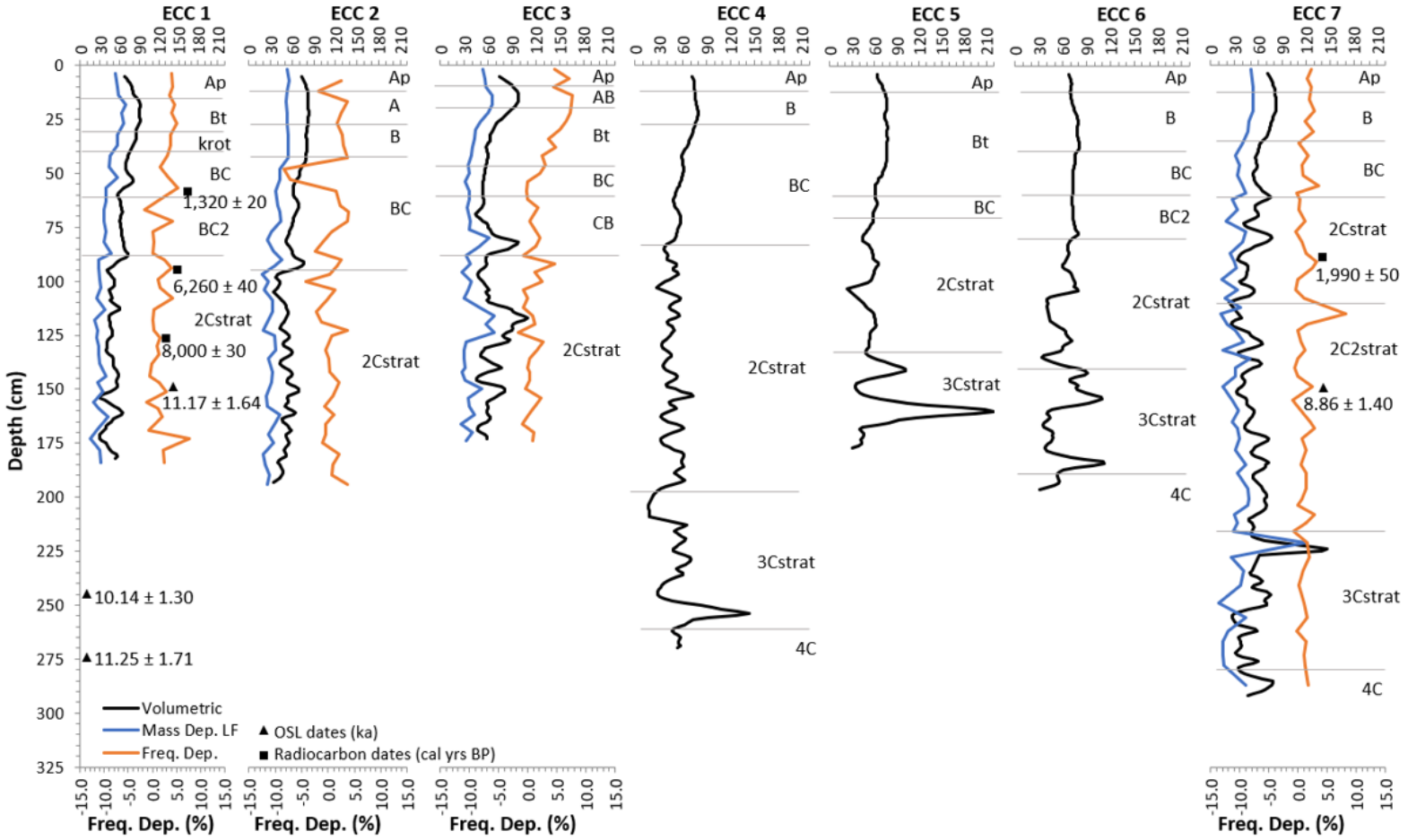

Figure 3.4. Volumetric and frequency dependent magnetic susceptibility and radiocarbon and OSL ages for ECC.

Percent frequency dependence at ECC is highly variable. Core 1 has frequency dependence ranging from ~3-5% in the upper 60 cm before oscillating between ~0-4% for the remainder of the core, except for one pronounced peak of 7.6% at 173 cm. Frequency dependence in core 2 is generally between ~0-3.6%, with a maximum value of 3.9% at ~70 cm. Core 2 has a large negative peak of -8.3% at 50 cm. The upper 50 cm of core 3 has the highest frequency dependence, with values ranging from 2.1-7.6%. Below 50 cm, values range between -1-2% for the remainder of the core except for a value of 4.7% at 92 cm. Core 7 was oscillatory, with frequency dependence between ~0-3% for the entire core except for a peak of 8.3% at 115 cm. These values indicate moderate magnetic enhancement due to pedogenesis in the upper unit, but little to no pedogenic enhancement in the underlying sand units.

3.4.3. Stable Carbon Isotopes

Stable carbon isotope analysis from Good-1 and ECC reveal similar trends, although $\delta^{13}C$ data at ECC are more variable (Figs. 3.5 and 3.6). At both stringers, $\delta^{13}C$ is highest near the surface and generally decreases with depth. Percent total organic carbon (TOC) is highest within the Ap and A horizons, declines rapidly within the upper 50 cm, and remains below 0.3% to depth in all cores. Overall, Good-1 has less negative $\delta^{13}C$ values and greater percent TOC than ECC.

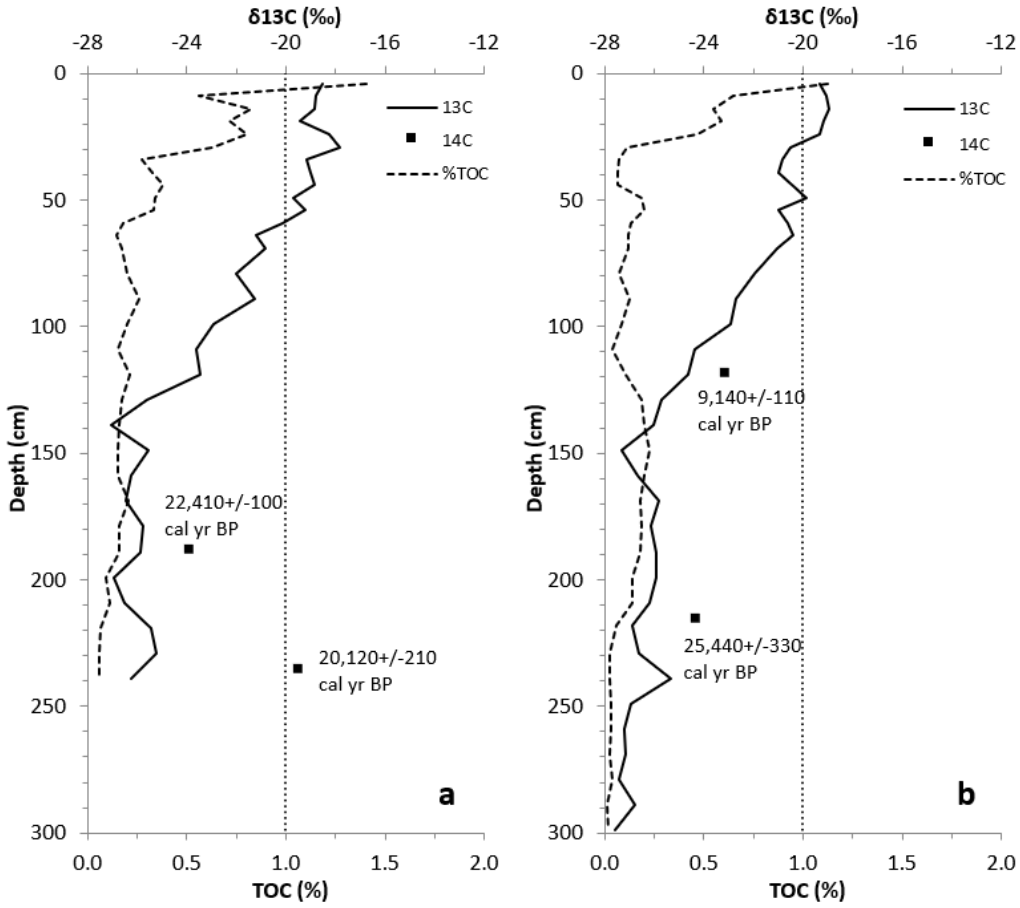

Figure 3.5. Stable carbon isotope analysis and radiocarbon ages from (a) Good-1 core 2 and (b) Good-1 core 4.

At Good-1, $\delta^{13}C$ values range from -17.8‰ to -27.0‰ in core 2, and from -18.9‰ to -27.6‰ in core 4 (Fig. 5). Stable carbon isotope values in core 2 range from only -17.8‰ to -18.6‰ in the upper ~50 cm (Ap, A, and B horizons) and then progressively decline to -27.0‰ at 139 cm (BC and C horizons). From 139 cm to 209 cm (C2 and 2C horizons), values fluctuate from -27.0‰ to -26.5‰ and then increase by 1.3‰ at 229

cm in the paleosurface unit (3C horizon) captured in the bottom 25 cm of the core. Core 4 exhibits similar trends in $\delta^{13}C$ values, ranging from only -18.9‰ to -19.35‰ in the upper ~25 cm (Ap and A horizons) and progressively declining to -27.3‰ at 149 cm (BC, C, and upper C2 horizons). From 149 cm to the base of the core at 299 cm (lower C2, 2C, 2Ck, and 2C2 horizons), $\delta^{13}C$ fluctuates between -25.4‰ to -27.6‰, with a 1.2‰ increase in the 2Ck horizon at 239 cm.

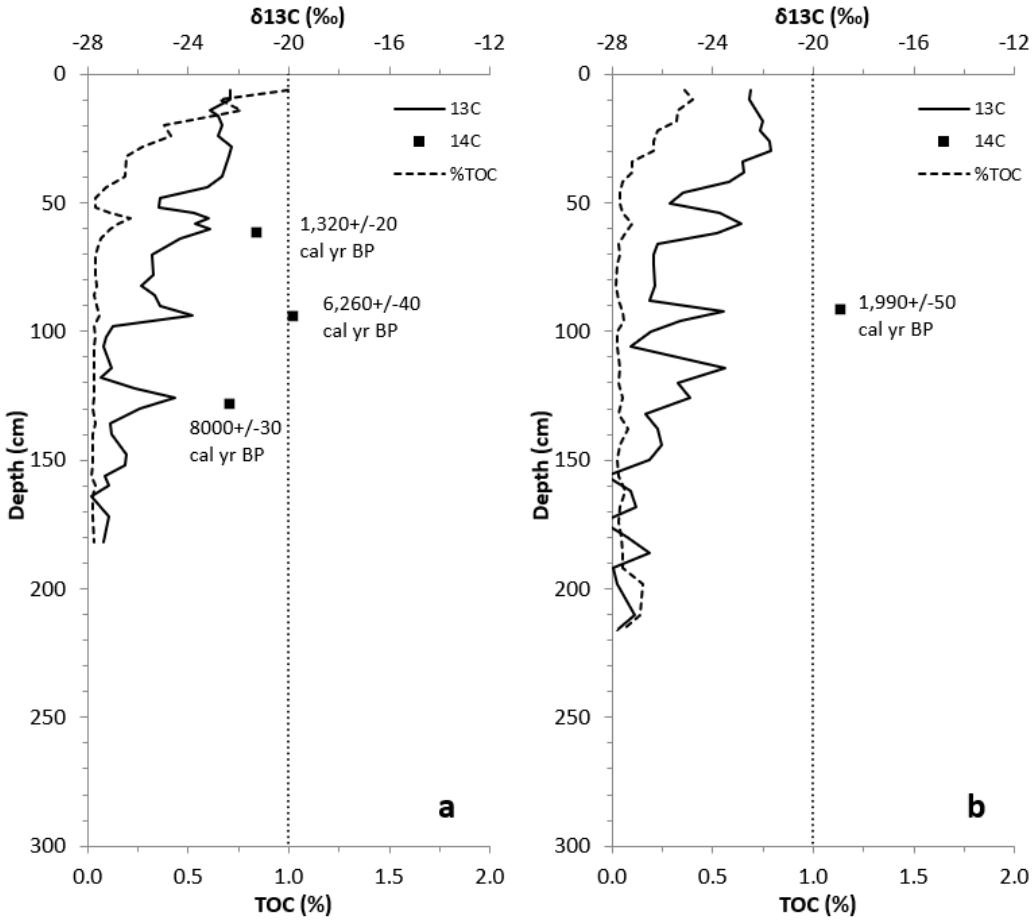

Figure 3.6. Stable carbon isotope analysis and radiocarbon ages from (a) ECC core 1 and (b) ECC core 7.

At ECC, $\delta^{13}C$ values range from -22.3‰ to -27.9‰ in core 1, and from -21.7‰ to -28.4‰ in core 7 (Fig. 3.6). The highest values occur within the upper sandy loam unit, and the lowest values are within the stratified units and basal unit. While there is a general trend of decreasing $\delta^{13}C$ values with depth, shifts of 1-3‰ in 4 cm intervals are common. Peaks in $\delta^{13}C$ occur within iron-cemented beds; however, several iron-cemented beds also have $\delta^{13}C$ values shifted towards more negative values.

In ECC core 1, $\delta^{13}C$ values range from -22.3‰ to -23.1‰ in the upper 40 cm (Ap and Bt horizons). From 40 cm to 52 cm, $\delta^{13}C$ declines to -25.2‰ and then increases to -23.6‰ at 60 cm, within an iron-cemented bed. Values then decline to -25.9‰ at 82 cm, increase to -23.8‰ at 94 cm within an iron-cemented bed, and then decline rapidly to -27.0‰ at 98 cm. Isotope values remain ~-27‰ to 118 cm, increase to -24.5‰ within an iron-cemented bed at 126 cm, decline to -27.1‰ at 136 cm, and fluctuate between -26.5‰ and -27.9‰ to 182 cm near the base of the core. Isotope values exhibit similar trends in ECC core 7, with $\delta^{13}C$ between -21.7‰ and -22.5‰ in the upper 30 cm, and values declining to ~-28‰ in the lowermost samples at ~220 cm. Positive shifts of 2.8‰ at 58 cm, 2.9‰ at 92 cm, and 3.6‰ at 114 cm occur within iron-cemented beds.

3.5. Discussion

Stratigraphy of Good-1 and ECC reveals Good-1 is more silt-rich and ECC is more sand-rich suggesting they formed from differing inputs of local sands and regional loess.

Good-1 is composed of an upper silt-rich unit, an underlying sand-rich unit, and a basal paleosurface unit (Table 3.3). The silt-rich unit is interpreted to be Peoria Loess, a fine-textured deposit that covers most of Goodhue County (Hobbs and Setterholm, 1998; Mason et al., 1994; Muhs et al., 2008). The sand-rich unit at Good-1 is interpreted as glacial outwash based upon its coarser grain size and the inclusion of occasional gravels. This is consistent with Goodhue County geologic maps that indicate glaciofluvial deposits and till make up the surficial deposits surrounding Good-1 (Hobbs and Setterholm, 1998). Only the upper 25 cm of the paleosurface unit was retrieved during coring, and details of its origin remain largely unknown; however, it is interpreted to predate the formation of Good-1 stringer given its darker color and finer grain size.

ECC stratigraphy consists of a surficial sandy loam unit, an upper stratified unit, a lower stratified unit, and a basal paleosurface unit (Table 3.4). The coarser grain sizes at ECC suggest more proximal sediment sources (Sun et al., 2002). The lower stratified unit is interpreted as being glacial outwash sands, which are widely distributed throughout Eau Claire County (Soil Survey Staff, 2019), specifically along the Chippewa River near ECC (Wisconsin DNR, 2011). The Chippewa River served as a glacial meltwater stream during the LGM (Faulkner et al., 2016). It is interpreted that the sandy loam unit and upper stratified unit are the main stringer body, composed primarily of reworked glacial outwash sands. Within the stratified units at ECC, the iron-cemented and iron-stained bands are reminiscent of ortstein or placic horizons

(Soil Survey Staff, 2014, 1999); however, iron bands have also been observed at distinct textural boundaries (Bockheim, 2014; Obear et al., 2014). Shifts in soil texture, found throughout ECC stringer, can lead to perched water and iron reduction at textural discontinuities, while subsequent drying results in iron re-oxidation (Bockheim, 2014). Only ~10 cm of the basal paleosurface unit was captured in some ECC cores. Like Good-1, more information is needed to better understand this unit, but it likely predates stringer formation based upon its fine grain size and darker color.

In general, Good-1 has higher volumetric and mass-dependent magnetic susceptibility values than ECC (Figs. 3.3 and 3.4). Good-1 also has higher magnetic susceptibility in its silt-rich upper unit than in the lower sand-rich unit and paleosurface. These data illustrate that coarser grain sizes have lower magnetic susceptibility, a relationship that has been noted by Dearing et al. (1996). Within the stratified units at ECC, susceptibility is highly oscillatory with peaks correlating with the bands of iron-cemented and iron-stained sand. Frequency dependent magnetic susceptibility, which can determine the influence of pedogenesis (Dearing, 1999), suggests moderate pedogenic influence (i.e., %FD = 2-10%) in the surface horizons with little to no pedogenic influence (i.e., %FD <2%) for the remainder of the cores. Frequency dependence at ECC is variable, suggesting low to medium pedogenic influence throughout the cores.

At both stringers, $\delta^{13}C$ is highest within the surface horizons and then decreases with depth (Figs. 3.5 and 3.6). Mean July temperature is one of the primary controls on C3 versus C4 dominance for a given location (von Fischer et al., 2008), and decreases in $\delta^{13}C$ can be correlated with decreases in temperature over time (Nordt et al., 2007). $\delta^{13}C$ values from this study suggest temperatures have followed a general increasing pattern over time. Data from Good-1 indicate climate was cool and the landscape was dominated by C3 vegetation during the late Pleistocene. A distinct negative shift at 139 cm in core 2 and 149 cm in core 4 may document impacts of the Younger Dryas. Following this distinct shift, isotope values indicate progressive warming and increased prevalence of C4 vegetation throughout the Holocene. At ECC, several peaks in $\delta^{13}C$ correspond to iron-cemented bands within the stringer. These could relate to periods of increased temperature or moisture, or they may be due to translocation and accumulation of younger carbon from the overlying sandy loam unit. This sand-rich deposit has high percolation rates, and the iron-cemented bands suggest significant translocation has occurred. However, further analysis is needed to determine the timing and processes responsible for the formation of these iron cemented zones.

3.5.1. Regional Paleoclimate and Sand Stringer Formation

3.5.1.1. Last Glacial Maximum ~26.5-19 ka

During the LGM, Good-1 and ECC were unglaciated, but proximal to the Laurentide Ice Sheet (LIS). Good-1 is ~65 km east of the Des Moines Lobe terminal moraine boundary, and ECC is ~50 km southwest of the Chippewa Lobe terminal moraine boundary. During the LGM, the region was sparsely vegetated (Birks, 1976; Chumbley et al., 1990; Grigal et al., 1976; Keen and Shane, 1990), cold, and dry (Birks, 1976; Clayton et al., 2001; Muhs and Zárate, 2001; Zanner, 1999), with permafrost present during the LGM leading up to the Pleistocene-Holocene transition (Clayton et al., 2001; Loope, 2012; Mason, 2015; Schaetzl et al., Submitted). Outwash sands from the glaciers were being deposited at this time (Faulkner et al., 2016; Syverson, 2007), but were most likely trapped within permafrost.

Based on radiocarbon ages, formation of the Good-1 sand stringer began during the LGM (Table 3.5). The paleosurface and base of the silt-rich unit returned ages between ~25.5-20 ka. These ages strengthen the interpretation that Peoria Loess is the main sediment source at Good-1 because Peoria Loess deposition occurred during and following the LGM (Leigh and Knox, 1994). The source of Peoria Loess was likely fine-grained materials from Wisconsinan glacial outwash plains (Mason et al., 1994). Stable carbon isotope analysis correlated with radiocarbon ages

(Fig. 3.5) returned $\delta^{13}C$ values indicative of colder temperatures at this time (Nordt et al., 2007).

3.5.1.2. Pleistocene-Holocene Transition ~11.7 ka

The Pleistocene-Holocene transition was a period of extreme climatic variability (Nordt et al., 2007). At that time, the LIS was receding, permafrost was melting, and coarser, glacial outwash sands were becoming available for aeolian transport (Clayton et al., 2001; Loope, 2012; Mason, 2015). The coarser sediment found at ECC coupled with the OSL ages (Table 3.6) suggest ECC began forming during the Pleistocene-Holocene transition. Increased sand in some cores at Good-1 suggest outwash sands may have been a minor sediment source for that stringer as well. Studies in central and northern Minnesota and northeastern Iowa have suggested spruce dominated woodland vegetation during this time (Birks, 1976; Chumbley et al., 1990; Grigal et al., 1976; Keen and Shane, 1990); however, vegetation was likely still sparse based on numerous studies detailing aeolian activity during the Pleistocene-Holocene transition (Arbogast et al., 2015; Colgan et al., 2017; Rawling et al., 2008; Zanner, 1999).

3.5.1.3. Early Holocene ~11.7-8.2 ka

Aeolian activity persisted into the Early Holocene (Arbogast et al., 2015; Colgan et al., 2017; Rawling et al., 2008; Schaetzl et al., 2018; Zanner, 1999) as climate continued to warm (Birks, 1976; Chumbley et al., 1990; Clayton et al., 2001; Grigal et al.,

1976; Keen and Shane, 1990; Ma et al., 2004). A mixed-coniferous deciduous forest has been cited as the main vegetation in central and northern Minnesota and northeastern Iowa at this time (Birks, 1976; Chumbley et al., 1990; Grigal et al., 1976; Keen and Shane, 1990), but vegetation was likely sparse enough to continue to promote aeolian activity. Radiocarbon and OSL ages (~8-11 ka) from Good-1 and ECC suggest the sand stringers were still active during this time. Stable carbon isotope values begin increasing during this interval indicating an increase in temperature (Nordt et al., 2007).

3.5.1.4. Middle Holocene ~8.2 ka to Present

Climate continued to warm during the Middle Holocene based upon a regional shift in plant communities to prairie vegetation (Chumbley et al., 1990; Keen and Shane, 1990), before temperature began decreasing and precipitation increasing in the Late Holocene (Chumbley et al., 1990; Keen and Shane, 1990). Stable carbon isotope data support this interpretation, with increasing isotope values towards the surface; disturbance of the surface due to agriculture and discrepancies in radiocarbon ages at ECC prevents a precise reconstruction of Late Holocene conditions. Studies have shown that most aeolian landforms stabilized by the Late Holocene (Keen and Shane, 1990; Zanner, 1999), and data from this study supports that conclusion. Magnetic susceptibility showed higher levels of pedogenic influence in the surface horizons, which indicates sand stringer stabilization. Well-developed soils with B horizons were identified in all cores from both sites, suggesting a prolonged period of stabilization

and pedogenesis over the last several hundred to several thousand years (Schaetzl and Thompson, 2015).

3.6. Conclusion

The timing of sand stringer formation differs between the two study sites by ~10 ka, but both formed contemporaneously with other regional landforms. Good-1 likely formed during the LGM correlating with the timing of Peoria Loess deposition (Leigh and Knox, 1994). Data suggests ECC formation began during the Pleistocene-Holocene transition, which correlates with other aeolian landform studies from the region (Arbogast et al., 2015; Colgan et al., 2017; Rawling et al., 2008; Schaetzl et al., 2018; Zanner, 1999). Based upon magnetic susceptibility data, pedogenesis could not keep pace with sediment deposition and did not dominate until more recently, suggesting sand stringers did not undergo periods of alternating accumulation and soil formation. Stable carbon isotopes generally decrease over time, indicating temperatures were colder than modern during the primary periods of sand stringer formation and evolution.

Despite their prevalence on the landscape in the Upper Midwest, little is known about the geomorphic and environmental histories of sand stringers. This study indicates that these landforms preserve unique records of environmental change from at least the Pleistocene-Holocene transition and potentially as far back as the LGM. Data

reveal that timing, stratigraphy, and processes of sand stringer formation and evolution are complicated and spatially variable. Future research should focus on using paleoenvironmental proxies and dating methods on new sand stringer sites throughout the region. Further work will help establish a better understanding of sand stringer activity and how it relates to the larger scale aeolian history of the Upper Midwest.

CHAPTER 4: CONCLUSION

4.1. Conclusions

Good-1 and ECC have morphologies comparable to other sand stringers described in the literature (i.e., ~1-10 m high, up to 100 m wide, up to several km long, and oriented northwest-southeast) (Koch and Walters, 2004; Mason et al., 1999; Millett et al., 2018; Schaetzl et al., 2018; Zanner, 1999). Their northwest-southeast orientation is indicative of a predominantly northwest wind regime at the time of formation and throughout their evolution based upon the findings of this study and prior studies (Koch and Walters, 2004; Mason et al., 1999; Millett et al., 2018; Schaetzl et al., 2018; Zanner, 1999). Stratigraphy, based on soil descriptions and particle size distributions, suggests sediment sources for Good-1 and ECC are different from one another. Good-1 is primarily composed of silt-rich, regional Peoria Loess with minor local sand inputs, while ECC is primarily composed of sand derived from local sources with minor regional loess inputs. Timing of formation for the two sand stringers differ as well. Radiocarbon ages collected at the base of Good-1 indicate formation during the LGM ~20-15 ka and predate ECC by ~10 ka, with OSL and radiocarbon ages at ECC suggest formation during the Pleistocene-Holocene transition ~12-10 ka. Paleoenvironmental proxy data reveal similar trends in environmental change for both Good-1 and ECC. Stable carbon isotopes generally decrease over time and temperatures were 2-3°C colder during sand stringer formation compared to modern conditions, and magnetic susceptibility data shows

higher levels of pedogenic influence in the surface horizons, indicating stabilization and pedogenesis dominated for at least the last several hundred centuries to millennia.

Paleoenvironmental proxy evidence coupled with sand stringer morphology, stratigraphy, and geochronology suggests the following:

- Following the LGM, glacial retreat resulted in outwash deposition across the Upper Midwest (Syverson, 2007), and westerly winds dispersed Peoria Loess throughout the region (Leigh and Knox, 1994), providing the main sediment source for Good-1; ECC had not yet begun to form.
- During the Pleistocene-Holocene transition, permafrost began to melt (Clayton et al., 2001; Loope, 2012; Mason, 2015; Schaetzl et al., Submitted), and outwash sands became available as the main sediment source for ECC and a minor sediment source for Good-1. Peoria Loess continued to provide the main sediment source for Good-1 and was a minor sediment source for ECC.
- In the Early Holocene to Middle Holocene sediment accumulation and sand stringer evolution at Good-1 and ECC continued as climate warmed. Many regional studies correlate this time period with extensive aeolian activity (Arbogast et al., 2015; Colgan et al., 2017; Hanson et al., 2015; Krist and Schaetzl, 2001; Rawling et al., 2008; Schaetzl et al., 2018).
- Throughout the Middle to Late Holocene, Good-1 and ECC stabilized and pedogenesis began to dominate; pedogenesis continued to outpace aeolian

deposition and erosion to present. Following stabilization, iron-cemented and iron-stained bands formed along textural discontinuities at ECC due to water infiltration and high iron content.

4.2. Future Work

Remote mapping shows that sand stringers are present across the landscape in the Upper Midwest (Koch and Walters, 2004; Marcou et al., 2019; Millett et al., 2018; Schaetzl et al., 2018; Zanner, 1999), but field studies on sand stringers have been limited. Prior to this study, only one other study investigated stringer stratigraphy in-depth (Zanner, 1999). While the data gathered for this thesis provides valuable insight into this relatively unknown landform, further research is still needed.

Good-1, ECC, and Canfield Creek stringer (Zanner, 1999) all exhibit different stratigraphy and basal ages, suggesting sand stringers are complicated features that vary spatially and temporally. This highlights the need for further stratigraphic studies on stringers throughout the Upper Midwest. Soil coring is a method that can provide important stratigraphic information, but it is limited when studying changes in stratigraphy across a sand stringer. Ground penetrating radar (GPR) is a non-invasive, non-disturbing technique that reveals sub-surface stratigraphy (Jol and Bristow, 2003). Using this method, a 3D model of sub-surface stratigraphy could be created for the entirety of a sand stringer to correlate stratigraphic units, understand how

stratigraphy changes across a stringer, and confirm the formative wind direction(s). GPR coupled with soil descriptions at future stringer sites would greatly improve understanding of sand stringer formation and evolution.

There is also a need for more robust dating on sand stringers across the region. Maximum limiting ages at Good-1 and ECC vary by ~10 ka, indicating formation began at considerably different times. Continued use of geochronological methods like radiocarbon and OSL will help to better constrain the timing of sand stringer formation, evolution, and stabilization. In addition, this thesis represents the first study to use sand stringers as a means for paleoenvironmental reconstruction. Additional Midwestern stringers should be analyzed using methods such as magnetic susceptibility and stable carbon isotopes to establish better understanding of the environmental history of the Upper Midwest since at least the LGM.

REFERENCES

Anderson, J.L., Grigal, D.F., 1984. Soils and Landscapes of Minnesota. Agric. Ext. Serv. Univ. Minn. 8.

Arbogast, A.F., Luehmann, M.D., Miller, B.A., Wernette, P.A., Adams, K.M., Waha, J.D., O'Neil, G.A., Tang, Y., Boothroyd, J.J., Babcock, C.R., Hanson, P.R., Young, A.R., 2015. Late-Pleistocene paleowinds and aeolian sand mobilization in north-central Lower Michigan. Aeolian Res. 16, 109–116. https://doi.org/10.1016/j.aeolia.2014.08.006

Birks, H.J.B., 1976. Late-Wisconsinan Vegetational History at Wolf Creek, Central Minnesota. Ecol. Monogr. 46, 395–429. https://doi.org/10.2307/1942564

Blott, S.J., Pye, K., 2006. Particle size distribution analysis of sand-sized particles by laser diffraction: an experimental investigation of instrument sensitivity and the effects of particle shape: Particle size distribution analysis of sands by laser diffraction. Sedimentology 53, 671–685. https://doi.org/10.1111/j.1365-3091.2006.00786.x

Bockheim, J.G., 2014. Ortstein and Placic Horizons, in: Soil Geography of the USA. Springer, Cham. https://doi.org/10.1007/978-3-319-06668-4_18.

Brown, B.A., 1988. Bedrock Geology of Wisconsin: West-Central Sheet. Wisconsin Geological and Natural History Survey.

Chumbley, C.A., Baker, R.G., Bettis, E.A., 1990. Midwestern Holocene Paleoenvironments Revealed by Floodplain Deposits in Northeastern Iowa. Science 249, 272–274. https://doi.org/10.1126/science.249.4966.272

Clark, P.U., Dyke, A.S., Shakun, J.D., Carlson, A.E., Clark, J., Wohlfarth, B., Mitrovica, J.X., Hostetler, S.W., McCabe, A.M., 2009. The Last Glacial Maximum. Science 325, 710–714.

Clayton, L., Attig, J.W., Mickelson, D.M., 2001. Effects of late Pleistocene permafrost on the landscape of Wisconsin, USA. Boreas 30, 173–188.

Clayton, L., Moran, S.R., 1982. Chronology of Late Wisconsinan Glaciation in the Middle North America. Quat. Sci. Rev. 1, 55–82.

COHMAP Members, 1988. Climatic Changes of the Last 18,000 Years: Observations and Model Simulations. Science 241, 1043–1052. https://doi.org/10.1126/science.241.4869.1043

Colgan, P.M., Amidon, W.H., Thurkettle, S.A., 2017. Inland dunes on the abandoned bed of Glacial Lake Chicago indicate eolian activity during the Pleistocene-Holocene transition, southwestern Michigan, USA. Quat. Res. 87, 66–81. https://doi.org/10.1017/qua.2016.13

Dearing, J.A., 1999. Environmental magnetic susceptibility: using the Bartington MS2 system. Chi Pub., Kenilworth.

Dearing, J.A., Hay, K.L., Baban, S.M.J., Huddleston, A.S., Wellington, E.M.H., Loveland, P.J., 1996. Magnetic susceptibility of soil: an evaluation of conflicting theories

using a national data set. Geophys. J. Int. 127, 728–734. https://doi.org/10.1111/j.1365-246X.1996.tb04051.x

Dunevitz, H., Epp, A., 1995. Natural Communities and Rare Species of Goodhue County, Minnesota. State of Minnesota, Department of Natural Resources.

Dyke, A.S., Moore, A.J., Robertson, L., 2003. Deglaciation of North America. Geological Society of Canada, Ottawa, Ontario, Canada.

Ehleringer, J.R., Cerling, T.E., 2002. Biological and Ecological Dimensions of Global Environmental Change: C3 and C4 photosynthesis, in: Munn, T. (Ed.), Encyclopedia of Global Environmental Change. Wiley, Chichester ; New York, pp. 186–190.

Evans, M., Heller, F., 2003. Environmental magnetism: principles and applications of enviromagnetics. Elsevier.

Faulkner, D.J., Larson, P.H., Jol, H.M., Running, G.L., Loope, H.M., Goble, R.J., 2016. Autogenic incision and terrace formation resulting from abrupt late-glacial base-level fall, lower Chippewa River, Wisconsin, USA. Geomorphology 266, 75–95. https://doi.org/10.1016/j.geomorph.2016.04.016

Goble, R.J., Mason, J.A., Loope, D.B., Swinehart, J.B., 2004. Optical and radiocarbon ages of stacked paleosols and dune sands in the Nebraska Sand Hills, USA. Quat. Sci. Rev. 23, 1173–1182. https://doi.org/10.1016/j.quascirev.2003.09.009

Grigal, D.F., Severson, R.C., Goltz, G.E., 1976. Evidence of eolian activity in north-central Minnesota 8,000 to 5,000 yr ago. Geol. Soc. Am. Bull. 87, 4.

Hanson, P.R., Mason, J.A., Jacobs, P.M., Young, A.R., 2015. Evidence for bioturbation of luminescence signals in eolian sand on upland ridgetops, southeastern Minnesota, USA. Quat. Int. 362, 108–115. https://doi.org/10.1016/j.quaint.2014.06.039

Hobbs, H., Setterholm, D.R., 1998. Surficial Geology and Thickness of Quaternary Sediments. Geol. Atlas Goodhue Cty. Minn. Minn. Geol. Surv. Cty. Atlas Ser. C-12.

Jacobs, P.M., Knox, J.C., Mason, J.A., 1997. Preservation and Recognition of Middle and Early Pleistocene Loess in the Driftless Area, Wisconsin. Quat. Res. 47, 147–154. https://doi.org/10.1006/qres.1996.1864

Jirsa, M.A., Boerboom, T.J., Chandler, V.W., Mossler, J.H., Runkel, A.C., Setterholm, D.R., 2011. S-21 Geologic Map of Minnesota - Bedrock Geology.

Jol, H.M., Bristow, C.S., 2003. GPR in sediments: advice on data collection, basic processing and interpretation, a good prectice guide, in: Ground Penetrating Radar in Sediments. Geological Society, London, pp. 9–27.

Keen, K.L., Shane, L.C.K., 1990. A continuous record of Holocene eolian activity and vegetation change at Lake Ann, east-central Minnesota. Geol. Soc. Am. Bull. 102, 12.

Koch, J., Walters, J.C., 2004. Late Quaternary eolian sand stringers of northeast Iowa. Presented at the Geological Society of America Annual Meeting.

Krist, F., Schaetzl, R.J., 2001. Paleowind (11,000 BP) directions derived from lake spits in Northern Michigan. Geomorphology 38, 18.

Larson, P., pers. comm. 2021. Aeolian Landforms in the Upper Midwest.

Leigh, D.S., Knox, J.C., 1994. Loess of the Upper Mississippi Valley Driftless Area. Quat. Res. 42, 30–40.

Lepper, K., Fisher, T.G., Hajdas, I., Lowell, T.V., 2007. Ages for the Big Stone Moraine and the oldest beaches of glacial Lake Agassiz: Implications for deglaciation chronology. Geology 35, 667. https://doi.org/10.1130/G23665A.1

Loope, H., 2012. Late Pleistocene eolian activity linked to permafrost degradation in the Upper Mississippi River basin, USA. Quat. Int. 279–280, 288. https://doi.org/10.1016/j.quaint.2012.08.765

Ma, L., Castro, M.C., Hall, C.M., 2004. A late Pleistocene-Holocene noble gas paleotemperature record in southern Michigan. Geophys. Res. Lett. 31. https://doi.org/10.1029/2004GL021766

Maher, B.A., 1998. Magnetic properties of modern soils and Quaternary loessic paleosols: paleoclimatic implications. Palaeogeogr. Palaeoclimatol. Palaeoecol. 137, 25–54. https://doi.org/10.1016/S0031-0182(97)00103-X

Marcou, N., Slade, A., Mataitis, R., Millet, J., Larson, P.H., Faulkner, D., Schaetzl, R.J., Bowen, M., Running, G.L., 2019. Sand Stringers in southeastern Minnesota and west-central Wisconsin: A Progress Report. Presented at the American Association of Geographers Annual Meeting.

Mason, J.A., 2015. Up in the refrigerator: Geomorphic response to periglacial environments in the Upper Mississippi River Basin, USA. Geomorphology 248, 363–381. https://doi.org/10.1016/j.geomorph.2015.08.004

Mason, J.A., Nater, E.A., Hobbs, H.C., 1994. Transport Direction of Wisconsinan Loess in Southeastern Minnesota. Quat. Res. 41, 41–51.

Mason, J.A., Nater, E.A., Zanner, C.W., Bell, J.C., 1999. A new model of topographic effects on the distribution of loess. Geomorphology 28, 223–236. https://doi.org/10.1016/S0169-555X(98)00112-3

McKee, E.D. (Ed.), 1979. A Study of Global Sand Seas. United States Department of the Interior, Washington, D.C.

Millett, J., 2019. Cliff-Top Dunes in the Lower Chippewa River Valley of West-Central Wisconsin. Thesis Minn. State Univ. Mankato 133.

Millett, J., Anzalone, C., Coonen, K., Jansen, E., Gardner, D., Larson, P.H., Running, G.L., Faulkner, D., Schirmer, R., 2018. Sandy aeolian deposition in southeastern Minnesota and western Wisconsin: A forgotten and poorly understood sandy aeolian landscape. Preliminary Results. Presented at the Association of American Geographers Annual Meeting.

Muhs, D.R., Bettis, E.A., Aleinikoff, J.N., McGeehin, J.P., Beann, J., Skipp, G., Marshall, B.D., Roberts, H.M., Johnson, W.C., Benton, R., 2008. Origin and paleoclimatic significance of late Quaternary loess in Nebraska: Evidence from stratigraphy,

chronology, sedimentology, and geochemistry. Geol. Soc. Am. Bull. 120, 1378–1407. https://doi.org/10.1130/B26221.1

Muhs, D.R., Zárate, M., 2001. Late Quaternary Eolian Records of the Americas and Their Paleoclimatic Significance, in: Interhemispheric Climate Linkages. Elsevier, pp. 183–216. https://doi.org/10.1016/B978-012472670-3/50015-X

Murray, A.S., Wintle, A.G., 2000. Luminescence dating of quartz using an improved single-aliquot regenerative-dose protocol. Radiat. Meas. 32, 57–73.

Noller, J.S., Sowers, J.M., Lettis, W.R., 2000. Quaternary Geochronology: Methods and Applications. American Geophysical Union.

Nordt, L., von Fischer, J., Tieszen, L., 2007. Late Quaternary temperature record from buried soils of the North American Great Plains. Geology 35, 159. https://doi.org/10.1130/G23345A.1

Nordt, L.C., Boutton, T.W., Hallmark, C.T., Walters, M.R., 1994. Late Quaternary Vegetation and Climate Changes in Central Texas Based on the Isotopic Composition of Organic Carbon. Quat. Res. 41, 109–120.

NRCS, 2006. Land Resource Regions and Major Land Resource Areas of the United States, the Caribbean, and the Pacific Basin. US Dep. Agric. Handb. 296, 682.

Obear, G.R., Hartemink, A.E., Soldat, D.J., 2014. Soils with iron-cemented layers on golf courses in the USA. Geoderma 232–234, 198–207. https://doi.org/10.1016/j.geoderma.2014.05.010

Peel, M.C., Finlayson, B.L., Mcmahon, T.A., 2007. Updated world map of the Köppen-Geiger climate classification. Hydrol. Earth Syst. Sci. Discuss. Eur. Geosci. Union 4, 439–473.

Poppe, L.J., Eliason, A.H., Hastings, M.E., 2003. A Visual Basic program to classify sediments based on gravel-sand-silt-clay ratios. Comput. Geosci. 29, 805–809.

Pye, K., Tsoar, H., 2009. Aeolian sand and sand dunes. Springer, Berlin.

Rawling, J.E., Hanson, P.R., Young, A.R., Attig, J.W., 2008. Late Pleistocene dune construction in the Central Sand Plain of Wisconsin, USA. Geomorphology 100, 494–505. https://doi.org/10.1016/j.geomorph.2008.01.017

Runkel, A.C., 1998. Geologic Atlas of Goodhue County, Minnesota: Bedrock Geology.

Schaetzl, R., Running, G., Larson, P., Rittenour, T., Yansa, C., Faulkner, D., Submitted. Luminescence Dating of Sand Wedges Constrains the Late Wisconsin (MIS-2) Permafrost Interval in the Upper Midwest, USA. Boreas.

Schaetzl, R.J., Forman, S.L., Attig, J.W., 2014. Optical ages on loess derived from outwash surfaces constrain the advance of the Laurentide Ice Sheet out of the Lake Superior Basin, USA. Quat. Res. 81, 318–329. https://doi.org/10.1016/j.yqres.2013.12.003

Schaetzl, R.J., Larson, P.H., Faulkner, D.J., Running, G.L., Jol, H.M., Rittenour, T.M., 2018. Eolian sand and loess deposits indicate west-northwest paleowinds during the Late Pleistocene in western Wisconsin, USA. Quat. Res. 89, 769–785. https://doi.org/10.1017/qua.2017.88

Schaetzl, R.J., Thompson, M.L., 2015. Soils: Genesis and Geomorphology, 2nd ed. Cambridge University Press, New York, NY.

Schoeneberger, P.J., Wysocki, D.A., Benham, E.C., Soil Survey Staff, 2012. Field Book for Describing and Sampling Soils, Version 3.0. National Resources Conservation Service, National Soil Survey Center, Lincoln, NE.

Soil Survey Staff, 2019. Soil Survey Geographic (SSURGO) Database. Natural Resources Conservation Service, United States Department of Agriculture.

Soil Survey Staff, 2014. Keys to Soil Taxonomy, 12th ed. USDA-Natural Resources Conservation Service, Washington, DC.

Soil Survey Staff, 1999. Soil taxonomy: A basic system of soil classification for making and interpreting soil surveys. 2nd edition. Natural Resources Conservation Service. U.S. Department of Agriculture Handbook 436.

Soil Survey Staff, N.R.C.S., United States Department of Agriculture, 2011. Official Soil Series Description - Mt. Carroll Series. URL https://soilseries.sc.egov.usda.gov/OSD_Docs/M/MT._CARROLL.html (accessed 12.30.20).

Soil Survey Staff, N.R.C.S., United States Department of Agriculture, 2007. Official Soil Series Description - Billett Series. URL https://soilseries.sc.egov.usda.gov/OSD_Docs/B/BILLETT.html (accessed 2.8.21).

Soil Survey Staff, N.R.C.S., United States Department of Agriculture, 2001. Official Soil Series Description - Kevilar Series. URL

https://soilseries.sc.egov.usda.gov/OSD_Docs/K/KEVILAR.html (accessed 12.30.20).

Stanley, K.E., Schaetzl, R.J., 2011. Characteristics and paleoenvironmental significance of a thin, dual-sourced loess sheet, north-central Wisconsin. Aeolian Res. 2, 241–251. https://doi.org/10.1016/j.aeolia.2011.01.001

Stuiver, M., Reimer, P.J., Reimer, R.W., 2021. CALIB 8.2 [WWW program]. URL http://calib.org (accessed 1.15.21).

Sun, D., Bloemendal, J., Rea, D.K., Vandenberghe, J., Jiang, F., An, Z., Su, R., 2002. Grain-size distribution function of polymodal sediments in hydraulic and aeolian environments, and numerical partitioning of the sedimentary components. Sediment. Geol. 152, 263–277. https://doi.org/10.1016/S0037-0738(02)00082-9

Syverson, K.M., 2007. Pleistocene geology of Chippewa County, Wisconsin. Wis. Geol. Nat. Hist. Surv. 62.

Tierney, J.E., Zhu, J., King, J., Malevich, S.B., Hakim, G.J., Poulsen, C.J., 2020. Glacial cooling and climate sensitivity revisited. Nature 584, 569–573. https://doi.org/10.1038/s41586-020-2617-x

University of Wisconsin - Extension, 2005. Bedrock Geology of Wisconsin. Geological and Natural History Survey.

University of Wisconsin - Extension, 1965. Early Vegetation of Wisconsin. Geological and Natural History Survey.

U.S. Climate Data, 2020a. Climate Eau Claire - Wisconsin. URL https://www.usclimatedata.com/climate/eau-claire/wisconsin/united-states/uswi0204 (accessed 12.30.20).

U.S. Climate Data, 2020b. Climate Red Wing - Minnesota. URL https://www.usclimatedata.com/climate/red-wing/minnesota/united-states/usmn0620 (accessed 12.30.20).

Vader, M.J., Zeman, B.K., Schaetzl, R.J., Anderson, K.L., Walquist, R.W., Freiberger, K.M., Emmendorfer, J.A., Wang, H., 2012. Proxy Evidence for Easterly Winds in Glacial Lake Algonquin, from the Black River Delta in Northern Lower Michigan. Phys. Geogr. 33, 252–268. https://doi.org/10.2747/0272-3646.33.3.252

von Fischer, J.C., Tieszen, L.L., Schimel, D.S., 2008. Climate controls on C3 vs. C4 productivity in North American grasslands from carbon isotope composition of soil organic matter. Glob. Change Biol. 14, 1141–1155. https://doi.org/10.1111/j.1365-2486.2008.01552.x

Wang, Y., Amundson, R., Trumbore, S., 1996. Radiocarbon Dating of Soil Organic Matter. Quat. Res. 45, 282–288. https://doi.org/10.1006/qres.1996.0029

Wisconsin DNR, 2011. Surficial Deposits. Ecol. Landsc. Wis. Handb.

Zanner, C.W., 1999. Late-Quaternary landscape evolution in southeastern Minnesota: Loess, eolian sand, and the periglacial environment. Dissertation, University of Minnesota.